ISRN LUTMDN/TMHP-17/5388-SE

ISSN 0282-1990

Efficiency and Emission Analysis of a Methanol Fuelled Direct Injection Spark Ignition Engine

Lee J. Björnestrand

Examensarbete på Civilingenjörsnivå
Avdelningen för Förbränningsmotorer
Institutionen för Energivetenskaper
Lunds Tekniska Högskola | Lunds Universitet

Efficiency and Emission Analysis of a Methanol Fuelled Direct Injection Spark Ignition Engine

Lee J. Björnestrand

April 2017, Lund

Föreliggande examensarbete på civilingenjörsnivå har genomförts vid Avd. för förbränningsmotorer, Inst för Energivetenskaper, Lunds Universitet - LTH. Handledare på LU-LTH: Assc. prof. Martin Tunér; examinator på LU-LTH: prof. Per Tunestål.

Examensarbete på Civilingenjörsnivå

ISRN LUTMDN/TMHP-17/5388-SE

ISSN 0282-1990

Avdelning för Förbränningsmotorer
Institutionen för Energivetenskaper
Lunds Universitet - Lunds Tekniska Högskola
Box 118, 221 00 Lund

www.energy.lth.se

Acknowledgements

This thesis was conducted at the division of combustion engines, a subsidiary to the department for energy sciences, at the university of Lund. Under the supervision of associate professor Martin Tunér, for whom I am very grateful to have received his expert guidance and assistance in this project. Also Sam Shamun, my daily supervisor, for helping me with the planning and execution.

My gratitude extends to the professors of the division and Ph.D students who have helped me with understanding the finer details and theoretical concepts of this subject. A special thanks must be made to Kenan Muric who provide, 'the spark', data post-processing and much more. He always had his door open for me and has shown great enthusiasm for this project. A big thank you to the technicians who solved all of the hardware issues with an abundance of patience and good humour.

Finally, but most importantly the biggest thank you is to my darling wife Louise, who has supported me mentally, emotionally (and financially), enabling me to fulfil my life's ambition of becoming a mechanical engineer.

“Smoke me a kipper…I’ll be back for breakfast!”

-Ace Rimmer

Abstract

With the signing of the Paris climate change deal of 2015, a global agreement was made to reduce anthropogenic greenhouse gas emissions. The maritime industry is currently investigating ways to reduce their carbon footprint. One such initiative is the SUMMETH (Sustainable Marine Methanol) project, spearheaded by the Swedish maritime agency.

The SUMMETH projects main aim is to investigate possible combustion concepts using methanol as a fuel. Methanol is a single carbon alcohol, the simplest of the chemical group. Methanol is a renewable fuel which can be produced through several different renewable processes, such as the gasification of wood.

This thesis investigates the efficiencies and emissions of the combustion concept DISI (direct injection, spark ignition) using methanol as the fuel on a heavy duty Scania engine, converted for single cylinder use. A compression ratio of 17.3:1, ambient air intake pressure and globally lean fuel: air mixtures were used.

Three experimental campaigns were carried out. Firstly, investigating the effect of spark timing, start of injection and common rail pressure. The second campaign investigated the effect of EGR (exhaust gas recirculation) on combustion. Finally, the third campaign utilised an MBT (maximum brake torque) spark timing in combination with EGR to further optimise engine operation.

The conclusions of the report are that; a larger range of operation is available at higher common rail pressures. There exists an optimum start of injection to spark timing separation. This separation is sensitive to EGR. Indicated gross efficiencies of 54% are possible with this combustion concept. An emission after treatment system would be necessary in order to comply with current emission legislation.

Table of Contents

List of Abbreviations, Acronyms and Definitions

ATDC = After Top Dead Centre

BTDC = Before Top Dead Centre

CAD = Crank Angle Degree

CFD = Computational Fluid Dynamics

CI = Compression Ignition

DI = Direct Injection

DISI = Direct Injection Spark Ignition

EGR = Exhaust Gases Recirculated

ICE = Internal Combustion Engine

MBT = Maximum Brake Torque

NTP = Normal Temperature and Pressure

RON = Research Octane Number

SI = Spark Ignition

TDC = Top Dead Centre

TWC = Three Way Catalyst

V_d = Displacement Volume

WOT = Wide Open Throttle

Chapter 1

1 INTRODUCTION

The Paris agreement of 2015 legally binds 195 countries in the first ever universal climate change deal. The main goals of this agreement are to limit the increase in global average temperature to well below 2^{o}C and reduce global emissions of anthropogenic greenhouse gases [1].

Within the maritime industry many initiatives are underway seeking to increase energy efficiency and advance the technological development of alternative fuels, in order to reduce their emissions and carbon footprint. The Sustainable Marine Methanol project, "SUMMETH", is one such project focusing on developing methanol as an alternative fuel for smaller marine vessels [2]. Testing and evaluating different methanol combustion concepts and identifying the GHG reduction potential for smaller marine engines, in the range of 250kW to 1200 kW, are the main goals in the SUMMETH project [2].

Methanol is considered to be one of the best alternative fuels for decarbonising the transport sector because it can be produced from a wide range renewable resources. Also when compared with other alternative transport energy carriers, methanol has a relatively high energy density. Methanol is also miscible with gasoline so blending successively higher amounts of methanol with gasoline provides the opportunity for a gradual transition to fossil-free fuels. This combined with utilising already existing supply infrastructures makes methanol a very desirable alternative fuel.

Methanol can be produced from forestry biomass, including the bi-products of the forestry industry, through a process known as the gasification of wood. This option has obvious benefits for a country such as Sweden. The relatively fast growth rate of trees would make methanol produced by wood gasification a renewable fuel, resulting in zero net CO_2 emissions [3].

Methanol can be synthesised by reacting, extracted atmospheric CO_2 with hydrogen produced from the electrolysis of water. This method results in a closed carbon loop and therefore burning this fuel will not increase the net amount of atmospheric CO_2. The electrolysis of water requires large amounts of electricity and for this reason fuels produced by this means are referred to as "electro-fuels" [4].

Methanol can also be obtained from the partial oxidation of biomass (from cereal crops) into syngas which then undergoes catalytic conversion into methanol [5]. However, fuels produced from this source of biomass in general are not seen as viable long term solutions for replacing fossil fuels. This is because over production could have a negative impact on land usage and therefore reduce global food resources.

The goal of this investigation is to find out whether methanol directly injected into the cylinder producing highly stratified combustion initiated by a spark is at all possible. If it is possible then what are the boundary conditions with regard to spark timing and fuel injection strategy? What effect will the addition of EGR have on this combustion concept? Finally, what emission levels are produced by this new type of combustion concept?

Chapter 2

2 THEORY

2.1 Mean Effective Pressure and Efficiencies

A breakdown of the different forms of energy in an internal combustion engine can be seen in the cascade diagram below, *Figure 1*. Each of these energy forms are then normalised by the engine displacement volume and number of crank revolutions per power stroke, giving a Mean Effective Pressure (MEP). Using mean effective pressures allows for an easy comparison to be made between different engines, regardless of size, number of cylinders, ignition method etc. Starting at the top, the width of *fuel MEP* represents the energy introduced at the beginning of the cascade in the form of chemical energy from the fuel. The energy loses are shown as arrows leading off towards the side. Finally, at the bottom of the cascade diagram is the remaining energy which has been converted to mechanical work by the engine.

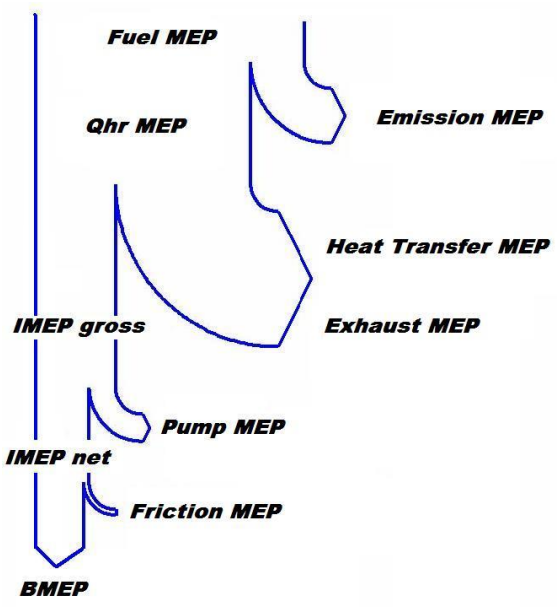

Figure 1 Sankey diagram of mean effective pressures.

- *Fuel MEP*. Total chemical energy injected into the cylinder at the beginning of the cycle.
- *Emission MEP*. Chemical energy losses due to incomplete combustion.
- *Qhr MEP*. *Thermal* energy remaining after losses due to incomplete combustion
- *Heat transfer MEP*. Energy losses in the form of radiation and convection heat transfer losses mainly through the cylinder walls.
- *Exhaust MEP*. Energy losses in the form of heat from the hot exhaust gases which are ejected out of the cylinder.
- *IMEP gross.* Gross indicated mean effective pressure.
- *Pump MEP*. Pumping loses through gas exchange. The loses are mainly caused through throttling of the intake gases.
- *IMEP net.* Net indicated mean effective pressure.
- *Friction MEP*. Energy loses due to mechanical friction in the engine, plus any remaining auxiliary losses.
- *BMEP*. Brake mean effective pressure. The useful mechanical energy which is converted into work after all of the energy losses have been accounted for.

The complete efficiency of an engine also known as the brake efficiency is the product of four separate efficiencies, seen below;

$$\eta_{brake} = \eta_{combustion}\,\eta_{thermodynamic}\,\eta_{gas\ exchange}\,\eta_{mechanical}$$

How these mean effective pressure are calculated and their relationship with engine efficiencies will be explained in the following section.

2.1.1 Fuel MEP

The initial injection of energy into the system in the form of chemical energy from fuel. This energy is equal to the mass of the fuel, m_f, multiplied with the lower heating value, Q_{LHV}, and then normalised by the displacement volume, V_d.

$$Fuel\ MEP = \frac{m_f\ Q_{LHV}}{V_d} \quad \text{Equation 1}$$

2.1.2 Q_{hr} MEP

Q_{hr} can be calculated from the heat release analysis. The amount of heat released is dependent upon how much of the fuel is burned in the cylinder and therefore is used with Fuel MEP to calculate combustion efficiency $\eta_{combustion}$. Q_{hr} is then normalised with the cylinder volume.

$$Q_{hr}MEP = \frac{Q_{hr}}{V_d} \quad \text{Equation 2}$$

$$\eta_c = \frac{Q_{hr}\ MEP}{Fuel\ MEP} \quad \text{Equation 3}$$

In this study the combustion efficiency will be measured through the gas analyser. This is regarded as a more accurate way to calculate Fuel MEP and subsequently Q_{hr} MEP [6].

2.1.3 IMEP $_{gross}$

The heat released through combustion and consequent expansion of the in-cylinder gases provides the work done on the piston, *W*. This work is expressed in the integral below;

$$W = \int p\ dV \quad \text{Equation 4}$$

This work, normalised with the displacement volume and measured from BDC at the beginning of the compression stroke to BDC at the beginning of the exhaust stroke, one crank revolution, gives rise to IMEP $_{gross}$.

$$IMEP_{gross} = \frac{1}{V_d} \int_{BDC}^{BDC} p\ dV \quad \text{Equation 5}$$

Thermodynamic efficiency, η_T, is then a measure of how much work is done from the heat released in combustion.

$$\eta_T = \frac{IMEP_{gross}}{Q_{hr}\ MEP} \quad \text{Equation 6}$$

2.1.4 Pump MEP

Gas exchange, the purging of exhaust gases and intake of new charge air, requires work from the engine. These pumping losses are counted as negative work, and normalised to give Pump MEP.

2.1.5 IMEP $_{net}$

The net indicated mean effective pressure is then a measure of the total work for a complete cycle, two crank revolutions, normalised by the cylinder volume. This then includes the work done during the compression and expansion stroke as well as the pumping work during the gas exchange. This can then be expressed as;

$$IMEP_{net} = IMEP_{gross} - Pump\ MEP \qquad \text{Equation 7}$$

For a four stroke engine such as in this investigation this is also expressed as;

$$IMEP_{net} = \frac{W_{compression} + W_{expansion} + W_{exhaust} + W_{inkake}}{V_d} \leftrightarrow \quad \text{Equation 8}$$

$$IMEP_{net} = \frac{1}{V_d} \int_{0\ CAD}^{720\ CAD} p\ dV \text{Equation 9}$$

Gas exchange efficiency, η_{GE}, is therefore a measure of how much work is lost through the exchange of exhaust gases (remaining from the combustion event during the previous cycle) for new intake gases needed for combustion during the current cycle.

$$\eta_{GE} = \frac{IMEP_{net}}{IMEP_{gross}} = \frac{IMEP_{gross} - Pump\ MEP}{IMEP_{gross}} = 1 - \frac{Pump\ MEP}{IMEP_{gross}} \qquad \text{Equation 10}$$

2.1.6 Friction MEP & BMEP

Friction mean effective pressure is used to group together, not only the mechanical losses which arise from piston ring friction and bearing friction etc. but also auxiliary systems required by the engine such as fuel pump, oil pump, water pump, generator etc. and any other losses. Since Friction MEP is used to account for all system losses it can only be calculated from brake mean effective pressure.

Brake MEP is then the final amount of work delivered from the engine measured on the dynamometer and normalised by the displacement volume. The mechanical efficiency, η_M, is then a measure of the energy losses associated with the engine itself. Which is expressed thus;

$$\eta_M = \frac{BMEP}{IMPE_{net}} = \frac{IMEP_{net} - Friction\ MEP}{IMEP_{net}} = 1 - \frac{Friction\ MEP}{IMEP_{net}} \qquad \text{Equation 11}$$

2.2 Rate of Heat Release

The first law of thermodynamics states that energy is neither created nor destroyed, it simply changes form. This conservation of energy can be applied to the engine cylinder as an ideal closed system. For a closed system the internal energy, U, is equal to the energy release from combustion, Q, minus the work done on the piston, W. The partial derivative of this relationship can be expressed thus;

$$\partial U = \partial Q - \partial W \qquad \text{Equation 12}$$

However, in reality there exists energy losses and therefore to improve the model, an open system is considered where the total energy released from combustion is broken down into; heat released, Q_{hr}, plus heat transfer loses, Q_{ht}, and crevice losses, Q_{cr}.

$$\partial Q = \partial Q_{hr} - \partial Q_{ht} - \partial Q_{cr} \quad \text{Equation 13}$$

The internal energy of the system can also be expressed thus;

$$U = mC_vT \qquad \text{Equation 14}$$

where m = mass

C_v = specific heat capacity for constant volume

T = temperature.

The partial derivative of internal energy can be expressed;

$$\partial U = m\partial u + u\partial m = mC_v\partial T + u\partial m \qquad \text{Equation 15}$$

An open system means that energy can leave the system but mass cannot, therefore δm=0.

Equation 15 can then be simplified to;

$$\partial U = mC_v\partial T \quad \text{Equation 16}$$

The work done by a gas is expressed;

$$\partial W = p\partial V \quad \text{Equation 17}$$

Where p = cylinder pressure

V = cylinder volume

Together with the ideal gas law: pV = mRT , where mass, m, is held constant and R is the gas constant, when written as partial derivatives;

$$\frac{\partial P}{P}\frac{\partial V}{V} = \frac{\partial T}{T} \quad \text{Equation 18}$$

$$\Leftrightarrow \partial T = T\left(\frac{\partial P}{P}\frac{\partial V}{V}\right) \quad \text{Equation 19}$$

Substituting *equation 19* into *equation 16* gives;

$$\partial U = mC_vT\left(\frac{\partial P}{P}\frac{\partial V}{V}\right) \quad \text{Equation 20}$$

equation 13 and *equation 17* substituted into *equation 12* gives;

$$\partial U = \partial Q_{hr} - \partial Q_{ht} - \partial Q_{cr} - p\partial V \quad \text{Equation 21}$$

equation 20 and *equation 21* together give;

$$\partial Q_{hr} - \partial Q_{ht} - \partial Q_{cr} - p\partial V = mC_vT\left(\frac{\partial P}{P}\frac{\partial V}{V}\right) \qquad \text{Equation 22}$$

From the ideal gas law $mT = \frac{pV}{R}$ inserted into *equation 22* gives.

$$\partial Q = \left(1 + \frac{C_v}{R}\right)p\partial V + \frac{C_v}{R}V\partial p + \partial Q_{ht} + \partial Q_{cr} \qquad \text{Equation 23}$$

For an ideal gas;

$R = C_p - C_v$ and $\frac{C_p}{C_v} = \gamma$ which together can be reformulated

to $1 + \frac{C_v}{R} = \frac{\gamma}{\gamma-1}$ Equation 24 and $\frac{C_v}{R} = \frac{1}{\gamma-1}$ Equation 25

equation 24 and *equation 25* can be substituted into *equation 23* to give;

$$\partial Q = \frac{\gamma}{\gamma-1}p\partial V + \frac{1}{\gamma-1}V\partial p + \partial Q_{ht} + \partial Q_{cr} \quad \text{Equation 26}$$

Finally, *equation 26* can expressed as a function of change in crank angle, thus;

$$\frac{\partial Q}{\partial \theta} = \frac{\gamma}{\gamma - 1} p \frac{\partial V}{\partial \theta} + \frac{1}{\gamma - 1} V \frac{\partial p}{\partial \theta} + \frac{\partial Q_{ht}}{\partial \theta} + \frac{\partial Q_{cr}}{\partial \theta} \qquad \text{Equation 27}$$

The above *equation 27* gives the rate of heat release, per crank angle degree. Expressed as a function of cylinder pressure, cylinder volume and their derivatives as a function of crank angle position. The ratio of specific heat capacity at constant volume and pressure must also be known. Additionally, for a complete solution to this equation the rate of heat loss, per crank angle degree, through the walls of the cylinder and the crevices must also be known.

2.3 Abnormal Combustion Phenomena

Knock occurs when the unburned mixture in front of the flame front auto-ignites causing high frequency pressure oscillations. If knock occurs late in the burning process, then the pressure oscillations are small. Knock favourable conditions often are related to advances in spark angle [7]. Knock is of particular interest in this study because it primarily occurs under wide-open throttle operation [8]. Resistance to knock is measure by the research octane number, where higher numbers correlate to greater knock resistance. Heavy knock is destructive to the engine and detrimental to efficiency.

Pre-ignition is flame initiation before the spark caused be surface ignition. Spark plugs, exhaust valves and carbon deposits are the most common sites for hot spots which lead to surface ignition. As with knock, pre-ignition can be destructive to the engine and is undesirable. Runaway pre-ignition, where pre-ignition occurs earlier and earlier and therefore more intensely can quickly lead to engine damage [9] [8].

2.4 Fuel Properties

By comparing some of the fuel properties for methanol, diesel and gasoline, whilst applying these differences with knowledge of combustion processes and the mechanics of an ICE, it is possible to evaluate the theoretical advantages of using methanol.

Table 1 Fuel properties [8]

Property	Methanol	Diesel	Gasoline
Density at NTP (kg/l)	0.79	0.82-0.95	0.74
Lower heating value (MJ/kg)	20.0	43.2	44.0
Heat of vaporisation (kJ/kg)	1103	270	350
Equivalence ratio for stoichiometric combustion	0.155	0.069	0.0685
RON number	106	-	91-99
Oxygen content by mass (%)	50	0	0

Comparing the density and lower heating value of methanol with gasoline and diesel it is apparent that to inject an equal amount of energy into the cylinder for each of these fuels, almost double the mass of methanol would be required as for the other two fuels.

Now comparing the heat of vaporisation for each fuel, methanol requires four and three times as much energy per unit mass as diesel respectively gasoline, to evaporate.

Combining therefore these two effects above, this leads to a charge cooling effect between six and eight times higher for methanol than for gasoline and diesel.

An increased RON leads to a greater available spark timing range.

Methanol is also an oxygenated fuel which should lead to increased fuel oxidisation.

2.5 Emission Gases

The complete combustion of a hydrocarbon fuel results in the products H_2O, CO_2, N_2 and O_2. This is not the case for an internal combustion engine, where the combustion is never complete which leads to harmful gases in the exhaust. Incomplete combustion of hydrocarbon fuels results in the following products; H_2O, H_xC_y, NO, NO_2, CO, CO_2. The formation of these emissions will be outlined below.

2.5.1 NOx

NOx is a group name given to both NO and NO_2, these gases are often grouped together because NO which is released into the atmosphere quickly oxidises into NO_2. The emission of these gases is controlled by law. NOx can be formed in three different ways. Thermal-, prompt- and fuel-NOx. Prompt-NOx is only of importance for conditions where thermal-NOx is not generated. Fuel-NOx can be produced when a fuel contains nitrogen, this does not apply to methanol. Thermal-NOx production is therefore the main formation process for this investigation.

Thermal-NOx is produced at high temperatures when there is an abundance of oxygen which reacts with the atmospheric nitrogen to produce NO. The formation rate is temperature dependant. Other factors which determine the amount of NOx formation are spark timing, lambda and EGR. At air/fuel ratios which produce lean or rich mixtures, NOx formation is low. The NOx formation levels increase towards stoichiometric mixtures as they produce higher flame temperatures and there is still oxygen present. The peak formation is at slightly lean mixtures. EGR can be used to reduce NOx formation because the exhaust gases have a higher specific heat capacity than air and are effective at reducing the combustion temperature thus lowering NOx levels. Spark timing can also be used to reduce NOx. Retarding combustion phasing by having the spark later leads to reduced combustion temperatures. Spark timing in combination with mixture dilution has been found to be very effective at reducing NOx emissions [6].

2.5.2 CO

Carbon monoxide engine emissions are also regulated by law. Although this gas is deadly in small doses, most CO emitted into the atmosphere will oxidise into CO_2. For that reason, CO regulations are not as strict as HC and NOx. The formation process for CO is quite simple, during combustion the hydrocarbon chain is broken down, there are many reactions which take place from the initial reactants and formation of the final products. Many different intermediate species are formed before they later go on to react again, finally the hydrogen atoms go on to produce water with oxygen, all of the carbon atoms oxidise to form first carbon monoxide and

then later oxidise again to form carbon dioxide. If there is insufficient oxygen or time for this two-stage reaction to complete, there will remain carbon monoxide.

2.5.3 CO_2

Carbon dioxide is known to be a greenhouse gas but as of yet the emission of this gas has not been regulated. Ways to reduce the emission levels of CO_2 are to;

1. Use a fuel with a high hydrogen to carbon ratio. Of the alcohol fuels methanol has the highest ratio.
2. Improve engine efficiency. This will reduce fuel specific CO_2 emissions.
3. Use a fuel with a short carbon cycle. Such as biofuels, as the carbon in the fuel was captured during photosynthesis. The time for the CO_2 released during burning of these fuels until it is recaptured in new plant growth and the cycle is closed is relatively short.

2.5.4 HC

Hydrocarbon emissions (HC) also known as unburned hydrocarbon emissions (UHC) and total hydrocarbon emissions (THC) are the third group of emission gases which are regulated by law for spark ignition engines. There is no formation process, the existence of hydrocarbons in the exhaust gases is purely a result of a combustion efficiencies less than unity.

Chapter 3

3 PREVIOUS STUDIES

As there are no known studies which investigate spark ignition, direct injection, methanol in a heavy duty engine. There exists no directly comparable study on which to base expectations. This literature study therefore evaluates four previous studies which were relevant to this investigation and shared some common aspects. A matrix was drawn up in order to compare similarities between this study and the four previous studies. This matrix is seen in .

Table 2 below. Where this study is referred to as SUMMETH. The full titles and list of authors names for the studies are as follows;

1. J. Vancoillie, J. Demuynck, L. Sileghem, M. Van De Ginste, S. Verhelst, L. Brabant and L. Van Hoorebeke, "The potential of methanol as a fuel for flex-fuel and dedicated spark-ignition engines," *Applied Energy,* vol. 102, pp. 140-149, 2013. [10]
2. M. J. Brusstar and C. L. Gray, Jr., "High Efficiency with Future Alcohol Fuels in a Stoichiometric Medium Duty Spark Ignition Engine," SAE Technical Paper, 2007-01-3993,2007. [11]
3. L. Sileghem, A. Ickes, T. Wallner and S. Verhelst, "Experimental Investigation of a DISI Production Engine Fuelled with Methanol, Ethanol, Butanol and ISO-Stoichiometric Alcohol Blends," SAE Technical Paper 2015-01-0768, 2015. [12]
4. M. Brusstar, M. Stuhldreher, D. Swain and W. Pidgeon, "High Efficiency and Low Emissions from a Port-Injected Engine with Neat Alcohol Fuels," SAE Technical Paper 2002-01-2743, 2002. [13].

Table 2 previous studies.

Study	PFI SI	DISI	Stoichiometric	Lean burn	Gasoline	Ethanol	Methanol	Light Duty	Heavy Duty	Boost	Compression Ratio
1	X		X	X	X		M100	X			10:1 19.5:1
2	X				X	E85	M85		X	X	16.3:1
3		X	X		X	E85 E100	M56 M100	X			11.3:1
4	X		X			E100	M100	X		X	19.5:1
SUMMETH		X		X			M100		X	X	17.3:1

The findings of these studies have been grouped into the following subjects for comparison.

3.1 Thermal efficiency

According to study 1 it is the fuel properties of methanol which make it such an interesting fuel to investigate. These properties lead to "superior" brake thermal efficiency [10]. High thermal efficiency for methanol is backed up by study 2 and study 4, which quantify peak brake thermal efficiency as >40% and 43% respectively. Both of these studies (2 & 4) also point out that brake thermal efficiencies of over 40% were found in a broad range of engine speeds and loads [11] [13]. Studies which have compared methanol with other alcohol fuels (gasoline, ethanol and butanol) have also found that methanol produces the highest thermal efficiency of all the fuels compared, in these studies [12].

All four studies explain the observation of high thermal efficiencies, for methanol fuelled engines, by the high heat of vaporisation for methanol. This leads to increased charge air cooling which leads to increased volumetric efficiency [10]. Study 2 also states that due to the high heat of vaporisation for methanol, the peak efficiency island is also broadened in comparison with E85 [11].

Study 3, which investigated direct injection and stoichiometric fuel/air mixtures, also credited methanol with a number of other smaller contributing factors to higher efficiency not present in other fuels. Such as, methanol has a higher burn velocity leading to a shorter burn duration and higher efficiencies. Burned methanol has a higher heat capacity which reduces the flame and exhaust temperatures. Lastly a higher specific heat ratio of C_p:C_v (also known as gamma, γ) might increase the expansion work [10].

3.2 Knock and pre-ignition

Another interesting property of methanol is resistance to self-ignition, which is indicated by an elevated RON number, around 109 [12]. A high RON number in combination with EGR, is the reason study 1 gave for being able to avoid abnormal combustion phenomena. Whilst making it possible to maintain optimal spark timing. EGR in this case was responsible for reducing cylinder temperatures [10]. The freedom for spark timing optimisation was also endorsed by study 4 which stated heavy dilution with EGR as the main reason for being able to reach MBT spark timing even at high loads with a high compression ratio of 19.5:1 [13].

The use of intake air temperature control, combined with a high heat of vaporisation allowed study 2 to avoiding pre-ignition. The study further explained that successful knock suppression at high compression ratios was accomplished with cooled EGR [11].

In a comparison with gasoline of RON number 97.1 study 3 noted that methanol achieved higher thermal efficiencies because the gasoline spark timings were "knock limited" [12].

3.3 Emissions

3.3.1 NOx Emissions

Common with all four studies is low levels of engine out NOx, due to lower combustion temperatures for methanol because of the increased charge cooling, reducing the unburned mixture temperature. Coupled with higher heat capacity of burned methanol reducing flame and exhaust temperatures. Study 1 reported consistently 5-10 g/kWh lower NOx with methanol compared to gasoline. How these two factors contributed to the reduction in NOx is not

clarified in the study [10]. Dilution with cooled EGR is also a trend in the studies, reducing NOx levels by causing a lower combustion temperature due to the higher heat capacity of exhaust gases compared with air [11] [13]. In study 3 internal EGR, i.e. exhaust gases which are not completely purged during the exhaust stroke and remain in the cylinder for the next cycle, were cited as the reason for low NOx levels with methanol [12].

Quantified specific engine out NOx levels were found to be as low as 3g/kWh (study 3) without additional EGR [12]. And even as low as 0.1-0.2 g/kWh with heavy dilution of EGR, around 50% (study 4) [13].

3.3.2 CO Emissions

In a comparison with gasoline, methanol was found to produce slightly lower specific CO emission (study 1). This is possibly due to methanol being an oxygenated fuel and therefore resulting in more complete oxidation [10]. These results were supported by studies 3 and 4 which found specific emission values (before TWC) around 16g/kWh and brake specific emission (after TWC) values of around 0.2g/kWh respectively [12] [13].

3.3.3 CO_2 Emissions

Specific CO_2 emissions found by studies 2 and 3 to be lower than ethanol by on average 3%, which was as low as 640 g/kWh [13] [12].

3.3.4 HC Emissions

With regard to hydrocarbon emission, study 1 reported a more complete combustion for methanol during lean operation leading to decreased unburned hydrocarbon and CO emissions [10]. These findings were reinforced in study 3 which found methanol to have the lowest HC emissions of all the fuels which were compared [12].

In study 4 an exhaust after treatment system was in place, presumably a three-way catalytic converter, which managed to keep brake specific hydrocarbon emissions to below 0.2 g/kWh over much of the range. [13]

3.4 EGR

As previously discussed, dilution with EGR is effective at reducing combustion temperature because it has a higher specific heat capacity than air and thus requires more energy to increase the temperature by the same amount, per unit mass. This was found to be advantageous in all studies for reducing NOx emissions and combustion abnormalities such as knock and pre-ignition. However, there is a limit to how much EGR can be applied before over dilution results in lower combustion efficiency and even unfired cycles. Study 1 found that up to 30% EGR could be applied before COV IMEPg exceeded 10%. The comparable amount of EGR for gasoline was 10%. Showing that methanol has a high potential for EGR dilution. [10] Supporting this finding, study 3 postulates that alcohol fuels have the potential for broadening the EGR working range due to high burning velocities [12]. EGR can also be used for load control as in study 4. The engine operated using stoichiometric fuelling, by moderating the intake manifold and EGR pressure, they were able to go between full load and almost idle conditions [13].

3.5 Compression Ratio

A range of compression ratios were employed on the four studies above, ranging from 10:1 to 19.5:1. The SUMMETH project originally planned to use a compression ratio of 20:1. However, after considering results from previous studies such as those mentioned here, it was decided to lower that to a more conservative 17.3:1, which is also the factory standard for this Scania direct injection compression ignition diesel engine.

Some of the disadvantages of a high compression ratio are that it increases chances of abnormal combustion phenomena. High in-cylinder temperatures lead to larger cooling loses to the cylinder wall and therefore lower efficiency. High in-cylinder temperatures also lead to increased NOx formation. [10] Study 2 claims that brake efficiency levels of a diesel engine maybe exceeded by using E85 or M85 and a compression ratio of 16.3:1 [13]

Chapter 4

4 HYPOTHESES

Before any experiment was conducted a list of hypotheses was drawn up. These hypotheses were based on knowledge gained from existing research and could later be compared with the experimental results and conclusions could be drawn. The hypotheses are listed below followed by the reasoning in italic text.

1. There will be an optimal separation between start of injection and ignition timing which will produce the highest efficiencies. *As fuel is injected into the cylinder, the fuel spray will pass by the spark plug electrode. The time at which the spark is delivered to this fuel spray will therefore be critical to combustion efficiency. Higher combustion efficiency will also lead to higher indicated efficiency.*

2. The start of injection and ignition timing combination which produces the highest indicated efficiencies will be different with the addition of EGR. *The addition of EGR will dilute the charge, causing prohibitive ignition conditions and affecting flame propagation as EGR levels increase. This will cause a reduction in combustion efficiency which in turn will lead to a reduction in overall indicated efficiency.*

3. Specific NOx emission will decrease with the addition of EGR. *The addition of EGR will dilute the charge with a gas which has a higher specific heat value than the air it replaces. This will result in lower combustion temperatures which in turn will curtail the conditions required for the formation of NOx.*

4. Specific hydrocarbon emissions will increase with the addition of EGR. *As stated above, charge dilution with EGR will reduce combustion efficiency leading to higher concentrations of unburned hydrocarbons in the exhaust gases.*

5. Emission after treatment will not be necessary for DISI methanol combustion combined with EGR and boost to fulfil current European emission legislation. *It is thought that a spark will be sufficient to ignite the charge without the need for heating the intake air. Additionally, EGR has a higher specific heat value than the air which is replaced. Therefore, compression of close ambient temperature charge with the addition of EGR is thought to be able to keep combustion temperatures low enough to produce below regulation requirement amounts of NOx. The oxygenated fuel will assist in oxidising CO to CO_2 thus generating low CO emissions. Soot emissions with alcohol fuels are ordinarily below emission regulations, both in terms of specific quantity and particle size. With regard to unburned hydrocarbon emissions, combustion will occur within the piston bowl combined with the direct injection strategy producing a non-homogenous charge thus negating crevice losses. These effects are thought to yield a higher combustion efficiency than normally attained with spark ignition combustion.*

6. Unburned hydrocarbon emission will be slightly higher than conventional compression ignition fossil fuel emission. *Although as stated above, combustion efficiency is expected to be higher than that ordinarily achieved with spark ignition combustion. It is not expected to be as high as conventional CI-fossil fuel combustion which is almost 100%.*

Chapter 5

5 EXPERIMENTAL SETUP

5.1 Test Cell Schematic

The test engine, mounted in a vibration damped rig within the test cell has connections to the air intake and exhaust system, as well as the drive shaft which is connected to the dynamometer. Mechanical power which is developed during fired cycles is delivered via the drive shaft to the dynamometer which is used to control the speed of the engine. During motored operation (unfired cylinder cycles) the dynamometer is used to provide power and keep a constant engine speed. A multitude of temperature probes and pressure transducers collect information from various locations in and around the engine. These include: in-cylinder, intake and exhaust manifold, as well as ambient (within the test cell), which are then displayed in the control room. The set up allows for full remote control of the engine speed, intake pressure and temperature, exhaust back pressure, EGR to air ratio control of the intake gases, common rail pressure control up to 2200 bar, up to three separate fuel injections each timed down to one micro second accuracy and spark timing timed to within one crack angle degree, all from the control room.

A schematic diagram illustrating engine, air intake and exhaust manifolds including the EGR control system in the test cell can be seen below in *Figure 2.*

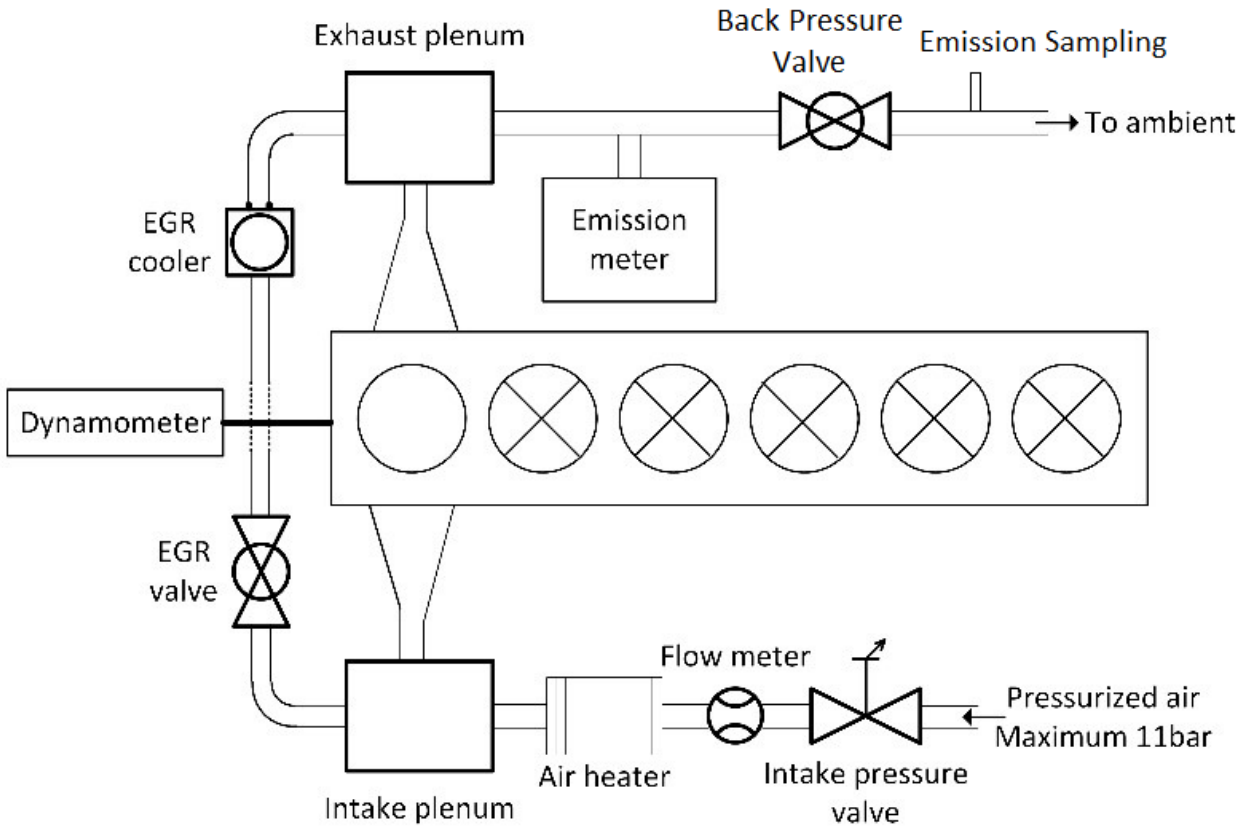

Figure 2 Setup schematic. [14]

5.2 The Test Engine

The engine to be used in the experiment is a modified Scania D13 heavy duty engine, comprising of six cylinders with a total displacement of thirteen litres. Modifications include; adaptations to operate with one active cylinder reducing the swept volume to 2.12 litres. A modified cylinder head to include an off-centre mounted spark plug. A drawing of the modified cylinder head can be seen below in *Figure 4*. Leaving the remaining five, non-fired, cylinders to be motored without compression. The compression ratio of the single fired cylinder was left as the factory standard for a diesel CI engine, 17.3:1. Details of the piston bowl geometry can be seen in *Figure* 3. The engine is equipped with an XPI common rail injection system as production standard, this enables a broad range of rail pressures. The fuel injector used is a ten hole, three hundred and twenty-five pounds per hour cup flow injector with an umbrella angle of one hundred and forty-eight degrees. This information is also displayed in *Table 3*.

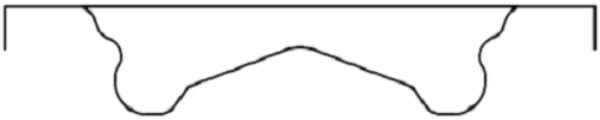

Figure 3 piston bowl geometry.

Table 3 Engine specifications

Engine specifications	
Swept volume	2124 cm^3
Stroke	160 mm
Bore	130 mm
Connecting rod	255 mm
Number of valves	4
Swirl ratio	2.1
IVC	-141 CAD ATDC
EVO	137 CAD ATDC
Injector specifications	
Injector model	XPI
Injector type	Solenoid
Spray angle	148º
Orifices	10
Flow rate	325 lb/h

5.3 Spark Plug Position

The cylinder head is modified to include the addition of a spark plug, illustrated below in *Figure 4.* The cylinder head is shown in green, fuel injector in red, and the spark plug mounting in white.

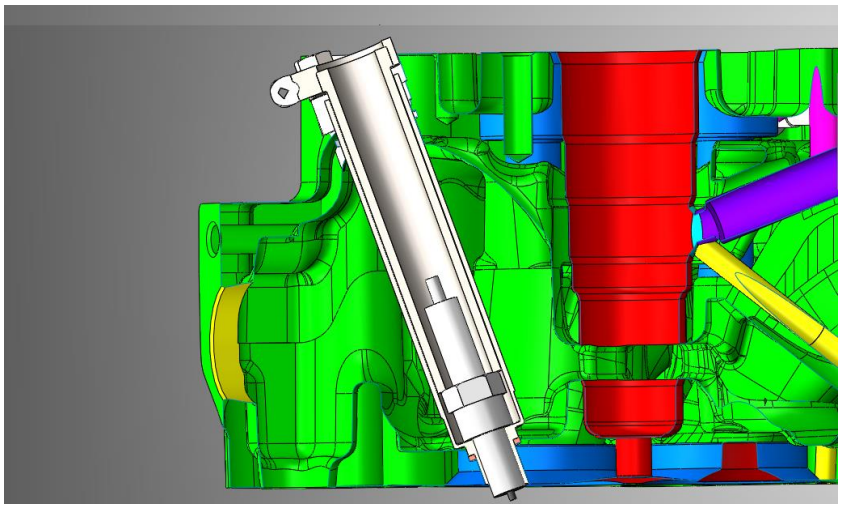

Figure 4 Position of spark plug.

The ignition system used is high energy system consisting of a high output IGBT (insulated-gate bipolar transistor) coil combined with an iridium tipped high performance spark plug. The location of the spark plug electrode in relation to the centre lines of the two adjacent fuels sprays is shown in the image below. The angle between two fuel sprays is thirty-six degrees and the spark plug electrode is 10.8º away from the centre line of the nearest spray.

Figure 5 Spark location between fuel sprays.

5.4 Gas Emission Analyser

The emission system which will be used to measure the emission gas constituents is an AVL AMA i60. Infrared detectors are used to measure CO and CO_2 both in the exhaust and intake manifold, for NOx and NO measurement a chemiluminescence detector is used, flame ionisation detector is used to quantify HC emissions, finally a paramagnetic detector is used to measure oxygen concentrations in the exhaust.

Chapter 6

6 METHOD

The experimental set up outlined in the previous chapter is to be used. The experiment is to be conducted and controlled from the control room, which has visual access via a window to the test cell for observational purposes. A computer terminal in the control room utilising the computer program Lab View will be used to facilitate the control and regulation of all variable experimental parameters, as well as providing real time displays of all sensor outputs. Lab View also contains software algorithms which can approximate values for $IMEP_{gross}$, COV $IMEP_{gross}$, $\eta_{combustion}$, heat release and Lambda in real time displays. Although these approximations of $IMEP_{gross}$, COV $IMEP_{gross}$, will be used for the purpose of carrying out the experiment, the exact values will later be calculated during the post processing of the pressure data. Only the post processed values will be used for the purpose of analysing the results. Combustions abnormalities will be detected visually, using the real time in-cylinder pressure trace displayed on the Lab View graphical user interface, and audibly by the experimenter.

6.1 Investigational Campaigns

This investigation into spark initiated combustion of methanol, directly injected into the cylinder on a heavy duty engine, was divided into three clear campaigns. These investigational campaigns were based upon the objectives of the investigation which were in turn designed to test the hypotheses.

6.1.1 Operational Sweep

The objective of the first campaign is to initiate stable combustion by means of a spark. This spark should provide sufficient activation energy to facilitate the chemical reaction between oxygen and methanol, to a degree that this reaction is able to propagate throughout the combustion chamber. Stable combustion in this case is defined as repeatable combustion cycles producing a covariance of $IMEP_{gross}$ less than or equal to ten. These cycles should also not include any detectable combustion abnormalities.

Once stable combustion is obtained three parameters will be altered independently to each other. These parameters are to be;

1. Common rail pressure. At 2000, 1500 and 1000 bar
2. Start of injection timing will begin at -30 CAD ATDC. This will then be retarded and advanced until limited by either combustion abnormalities or unstable combustion.
3. Spark timing will be advanced to -8 CAD ATDC and retarded to TDC, if this is achievable.

The fuel injection duration is to be altered to maintain a constant load on the engine. The intake air pressure and temperature is to remain constant throughout this campaign. No amount of EGR or exhaust back pressure will be applied during this campaign. This first campaign of testing is designed to validate the first two hypotheses.

6.1.2. The Effect of EGR

The second campaign will be to test hypotheses 2, 3, 4, and 5. EGR will be added in increasing amounts whilst, load, start of injection and spark ignition timings will be held constant. For the third campaignt, the same EGR sweep will be carried out again however this time spark timing will be varied in order to optimise efficiency. EGR will be increased at intervals of approximately 5% until combustion is no longer sustainable.

Chapter 7

7 RESULTS AND DISCUSSION

This chapter presents the results obtained during the experimental section of the investigation, together with a discussion which endeavours to provide an explanation of the results based on current combustion theories. This chapter is divided into three sections corresponding to the three experimental campaigns.

7.1 Knock

First it should be pointed out that the operational sweeps in this study were mainly limited by knock. The pressure traces which are displayed in the coming sections are mean pressure traces recorded over three hundred cycles and are unfiltered. When knock was detected during the experiment, the severity quickly escalated to severe knock. Presumably due to hot spots in the combustion chamber. The course of action was therefore to retard the ignition or in worst case, terminate the fuel injection if the knock did not subside. For this reason, there is very little recorded data including knock.

7.2 Operational Sweep

7.2.1 Common Rail Pressure 2000 bar

Parameter	**Value**
Common rail pressure	2000 bar
Engine Speed	1200 RPM
Lambda	1.5
Intake Temperature	85 ºC
Intake Pressure	1 bar
Exhaust Pressure	1 bar

Operational sweep at a load of 8 bar $IMEP_{gross}$. Spark timing varied between -6 to -2 CAD at intervals of 2 CAD. Start of injection varied from -56 to -23 CAD. Each blue ring on the chart represents a combination of spark timing and start of injection where it was possible to maintain stable combustion. There appears to be two distinct groupings of points; the first group being in a similar location to that as observed at lower rail pressures. These are the points at spark timing -6, -4, and -2 CAD, also spanning start of injection between -40 and -23 CAD. See *Figure 18* and *Figure 29*. The second group of points, which makes this chart different to the charts produced at lower rail pressures, is found at ST = -6 and SOI between -56 and -44 CAD.

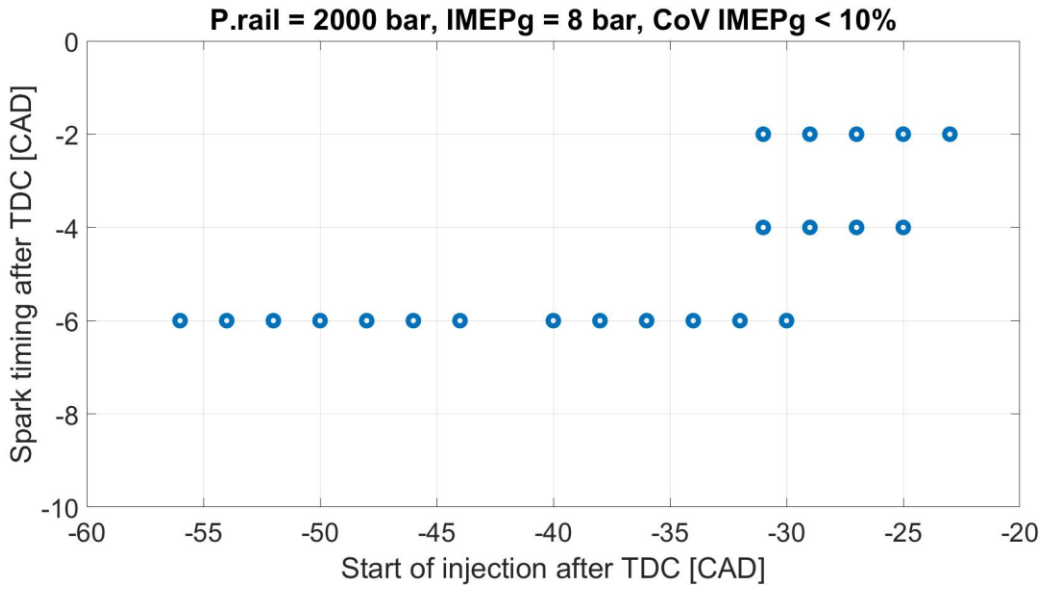

Figure 6 Operational points at 2000bar rail pressure

One explanation as to why this second group of points exists, at this common rail pressure only, is that high common rail pressure enables more air entrainment into the fuel spray. Making it possible to achieve stable combustion at a larger separation between SOI and ST, than was seen at other operational sweeps at lower common rail pressures.

Just to illustrate this point more clearly, below is a plot of the operational points at all three rail pressures *Figure 7*. Where blue circles indicate P.rail = 2000 bar, red circles indicate P.rail = 1500 bar and black circles indicate P.rail = 1000 bar.

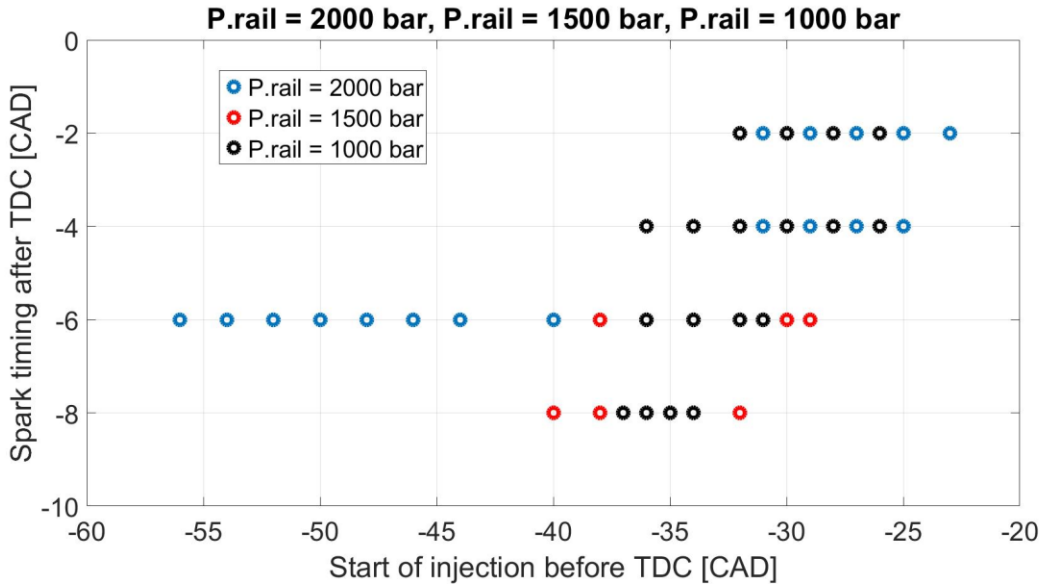

Figure 7 Operational points at all rail pressures.

Now a clear grouping of points can be seen between SOI = -40 to -23 CAD BTDC and ST = -8 to -2 CAD BTDC. Also the extra group of points which only appears for rail pressure at 2000 bar, this is at SOI = -56 to -44 CAD BTDC.

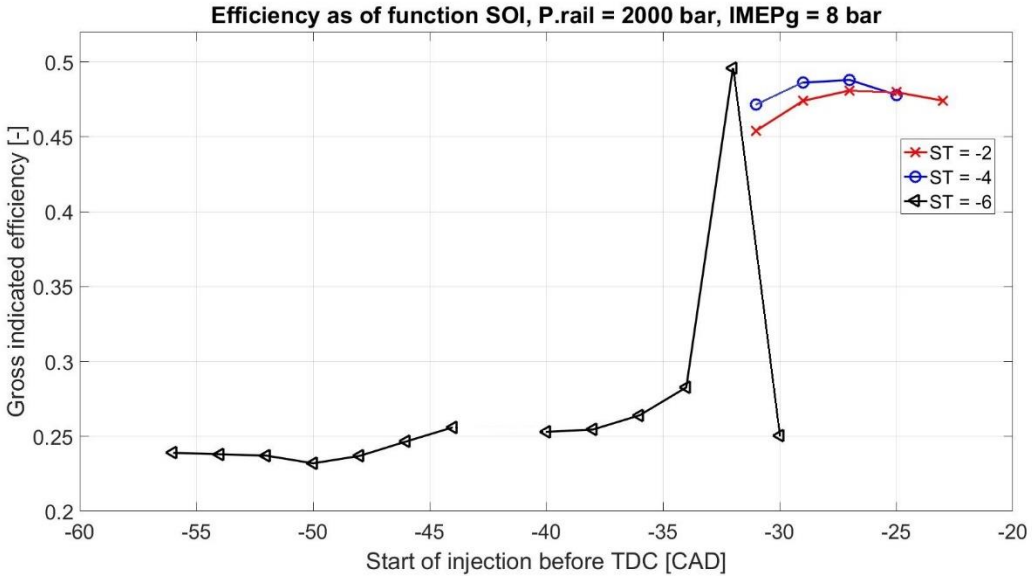

Figure 8 $\eta_{Gross\ Indicated}$; P_{rail} =2000 bar, $IMEP_g$ = 8 bar

Looking at the gross indicated efficiencies (*Figure 8*) for these operational points, at P.rail = 2000bar, where colours are used to group points with the same spark timing.

Firstly, the group of points with ST = -2, coloured in red. As the SOI is swept from -31 to -23 CAD, the gross indicated efficiency increases approaching SOI = -27 CAD then decreases after SOI = -27. Producing an apparent curve, where the maximum of this curve is at point ST = -2 SOI = -27, where the gross indicated efficiency is 48.1%. This would appear to be the optimal start of injection to spark timing separation of 25 CAD at ST = -2.

Secondly, the group of points with ST = -4, coloured in blue. As the SOI is swept from -31 to -25 CAD, the gross indicated efficiency, again increases approaching SOI = -27 CAD then decreases after SOI = -27. Producing an apparent curve, where the maximum of this curve is point ST = -4 SOI = -27 and the gross indicated efficiency is 48.8%. This would appear to give the optimal separation a value of 23 CAD at ST = -4.

Finally, the points marked in black with ST = -6. The only apparent trend here is that all but one of these points has remarkably lower efficiency than observed on the previous two sweeps. As will be discussed later in the report this is due to an apparent fuel leak.

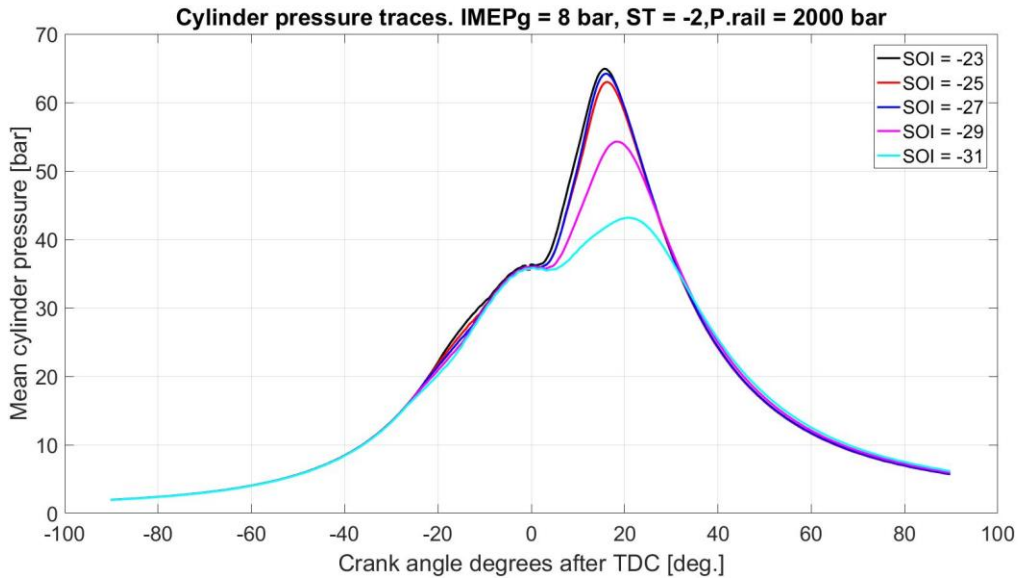

Figure 9 Mean cylinder pressures; P_{rail} =2000 bar, $IMEP_g$ = 8 bar, ST = -2 CAD ATDC

Figure 9 Shows the mean cylinder pressure traces for the SOI sweep relating to the data points at ST = -2. What is noticeable is the highest peak cylinder pressure is for SOI = -23 which was not the data point with the highest indicated efficiency. Another area of interest is between 25 and 15 CAD before TDC, this is where the fuel is injected. Here the different pressure traces separate from each other before converging again shortly before the combustion event. This separation is due to the evaporation of the fuel which has a cooling effect thus dropping the cylinder pressure. The overall shape of the pressure traces for combustions events corresponding to SOI = -23, -25 and -27 is synonymous to that which would be expected for higher efficiencies. That is to say these three traces reach higher peaks and have a lessened base.

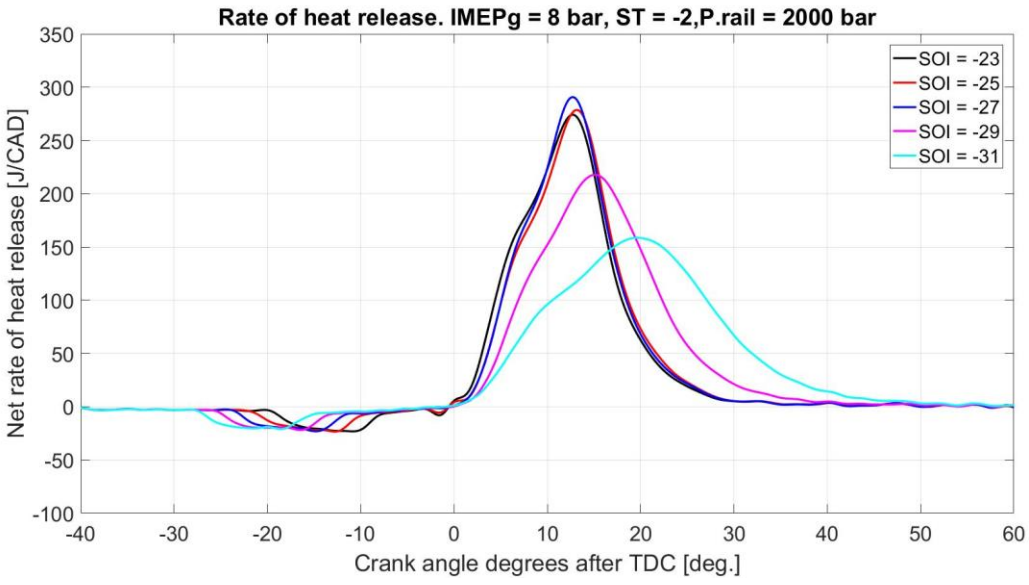

Figure 10 Heat release plots; P_{rail} =2000 bar, $IMEP_g$ = 8 bar, ST = -2 CAD ATDC

Figure 10 shows the rate of heat release plots for start of injection sweep at spark timing 2 CAD before TDC. Here the relationship with indicated efficiency is more pronounced. It is observed that the shape of the heat release curves for SOI = -23, -25 and -27 are very similar to each other. They have a base height proportionality which would be expected for higher efficiencies. That is to say the height is larger in proportion to the base. This implies a faster burning which means the energy is delivered under a shorter period of expansion, this is more favourable with respect to efficiency. However, faster burn rate leads to higher cylinder temperatures which can lead to greater heat transfer losses. The trace with the highest peak is at SOI = -27 CAD which also is the data point with highest indicated efficiency.

Fuel evaporation is more pronounced in the rate of heat release plots above than it was with the cylinder pressure traces. Here it is also possible to discern the different fuel injection timings. It should be pointed out that this phenomena is not usually seen in non-alcohol fuels and is associated with the elevated heat of vaporisation for methanol coupled with a low lower heating value which is seen in *Table 1*.

Another observation in the shape of the heat release curve which is apparent on all of the data points throughout the experiment, and which appears to be unique to this combustion concept, is decrease in the rate of heat release which creates a 'shoulder' on the left flank of the curve. It is hypothesised that this decrease in the rate of combustion could be due to the form of the piston bowl. Further CFD analysis or optical studies is required in order to confirm this theory.

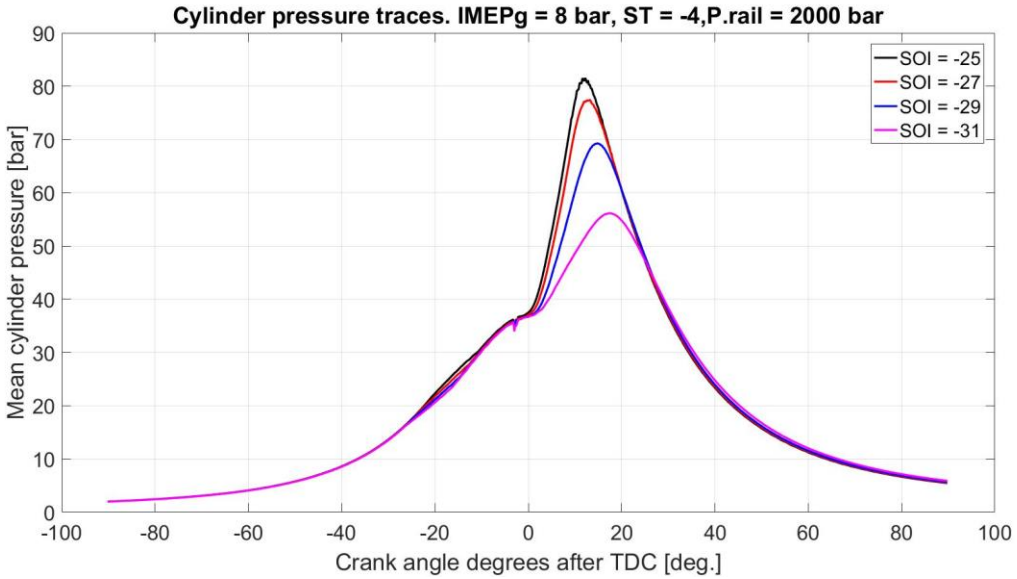

Figure 11 Mean cylinder pressures; P_{rail} =2000 bar, $IMEP_g$ = 8 bar, ST = -4 CAD ATDC

Figure 11 above shows the mean cylinder pressure traces for the start of injection sweep carried out at spark timing 4 CAD BTDC. As observed in *Figure 8* this sweep showed higher efficiencies at SOI = -27 and -29 CAD than all points at on the sweep at 2 CAD BTDC. The peak cylinder pressures for these points are higher, approximately 77 and 69 bar respectively, which is also higher than the highest peak cylinder pressure recorded in the previous sweep. Data point SOI = -25 CAD shows the highest peak cylinder pressure so far at over 80 bar. Also

visible in cylinder pressure traces is a spike which coincides with the spark timing. This is assumed to be only electrical interference and not an actual pressure spike.

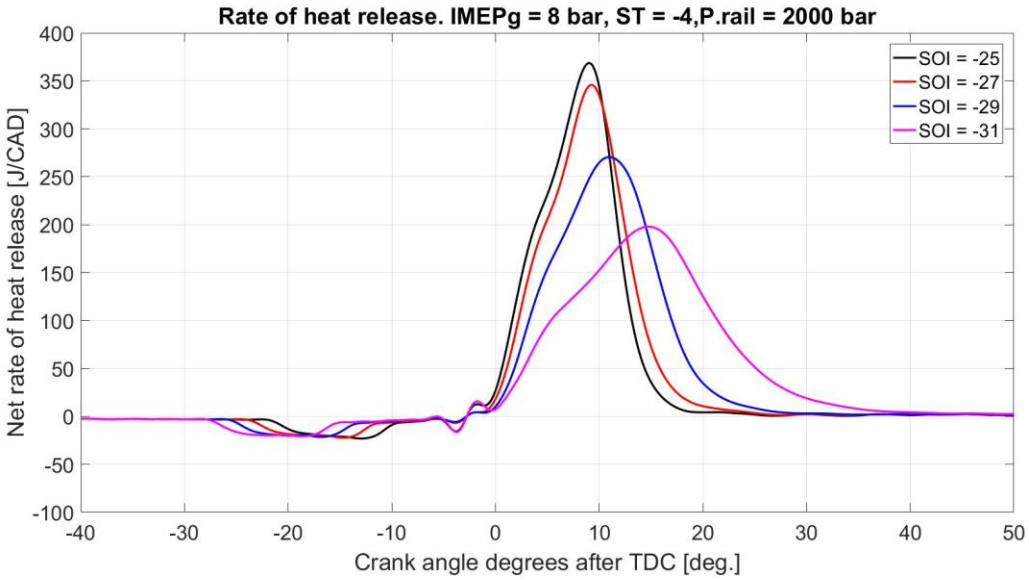

Figure 12 Heat release plots; P_{rail} =2000 bar, $IMEP_g$ = 8 bar, ST = -4 CAD ATDC

Comparing the heat release plots in *Figure 12* they all have good proportionality which would be expected from the relatively high efficiencies recorded. Again the cooling effect as the fuel evaporates is apparent, as is the 'shoulder' on the left flank of the curve. The most noticeable feature of this plot and the mean cylinder plot above (*Figure 11*) is that SOI = -25 would be expected to have a higher indicated efficiency than the other points. Because SOI = -25 reaches a higher peak cylinder pressure, additionally the heat release curve has a narrower base and reaches a higher peak rate of heat release, but this is not the case. This could be due to increased heat transfer losses, as previously described.

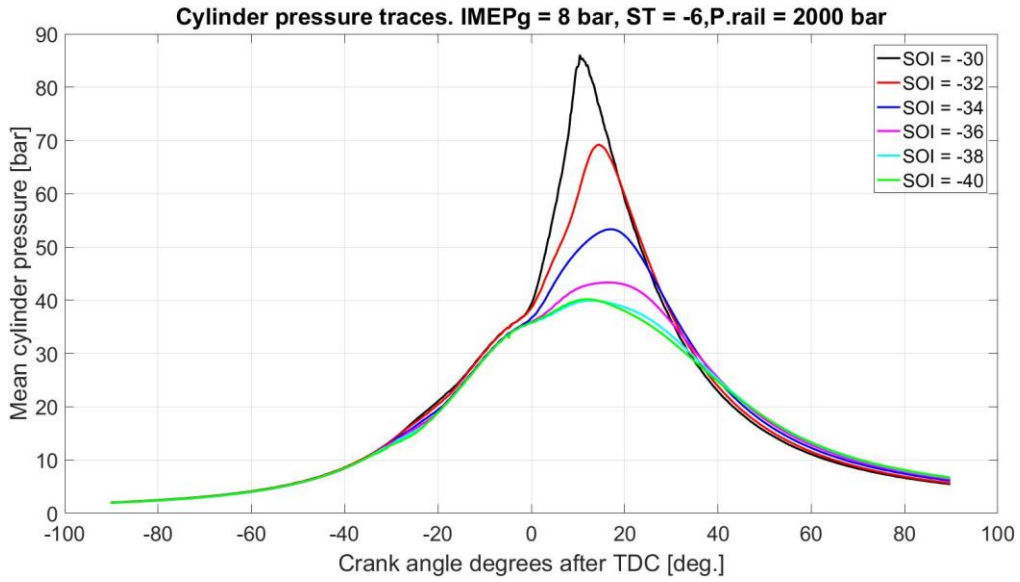

Figure 13 Mean cylinder pressures; P_{rail} =2000 bar, $IMEP_g$ = 8 bar, ST = -6 CAD ATDC, SOI = -30 to -40 CAD ATDC

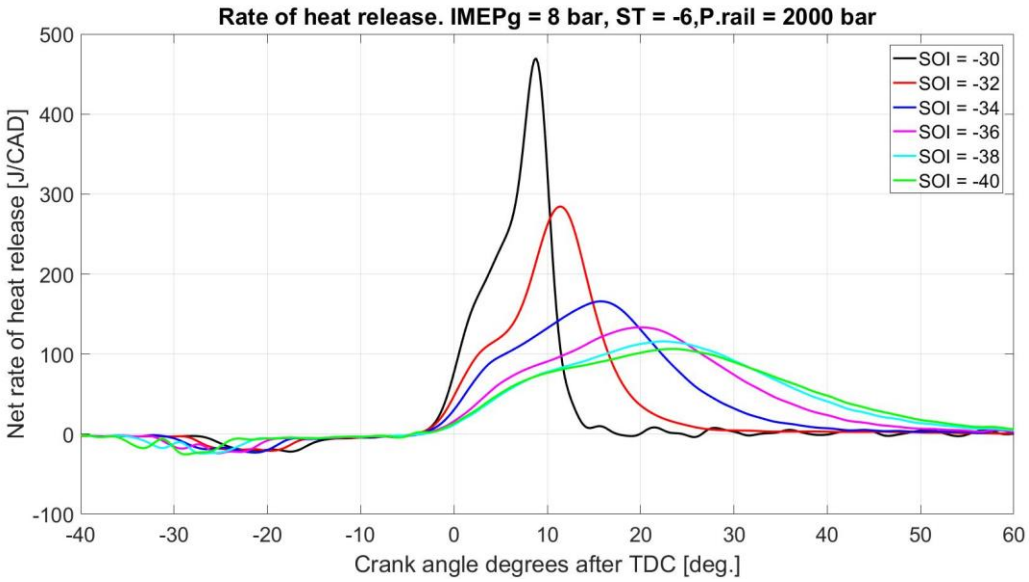

Figure 14 Heat release plots; P_{rail} =2000 bar, $IMEP_g$ = 8 bar, ST = -6 CAD ATDC, SOI = -30 to -40 CAD ATDC

Comparing the mean cylinder pressure traces for these points at ST= -6 with the other sweeps at ST = -2 and ST = -4 it would seem strange that the corresponding efficiencies are so low. For peak mean cylinder pressure over 50 bar and a peak rate of heat release approaching 200 J/CAD, an indicated efficiency of 45% would be expected. Note also that the point with the highest efficiency in the ST = -6 sweep is at SOI = -32, whereas comparing the mean cylinder pressure and rate of heat release trace for ST = -6 between SOI = -30 to -40, it would appear as though the point SOI = -30 should have a higher efficiency than point SOI = -32. This is expected because the peak mean cylinder pressure is higher and the rate of heat release has a narrower base and a higher peak, thus the heat is released over a shorter expansion duration. Although as seen in the previous sweep it was not the data point with the 'best' heat release

curve or highest peak cylinder pressure which resulted in the highest efficiency, possibly due to heat transfer losses.

Therefore, if the red line at SOI = -32 is assumed to have the highest efficiency, this would give the optimal separation as 26 CAD.

Plotting the fuel flow as a function of start of injection for these points and comparing with the plot of indicated efficiency as a function of start of injection, reveals an apparent fuel leak in the system. See *Figure 15*. This was also confirmed by a comparison of pump duty at similar points. This showed that the high pressure fuel pump was in fact working harder than usual to maintain the same fuel pressure in the common rail.

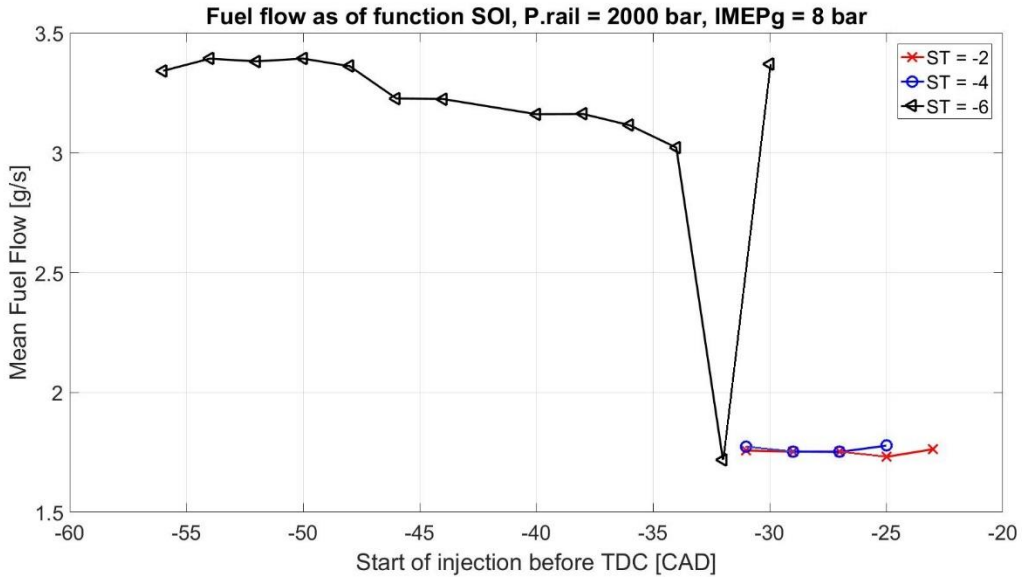

Figure 15 Fuel flow

Since the indicated efficiency is dependent upon fuel consumption the fuel leak has drastically reduced the indicated efficiencies for these points. Fuel flow is proportional to rail pressure and injection duration; therefore, it should be possible to correct for this error. It was decided not to do this as the results could not be considered reliable.

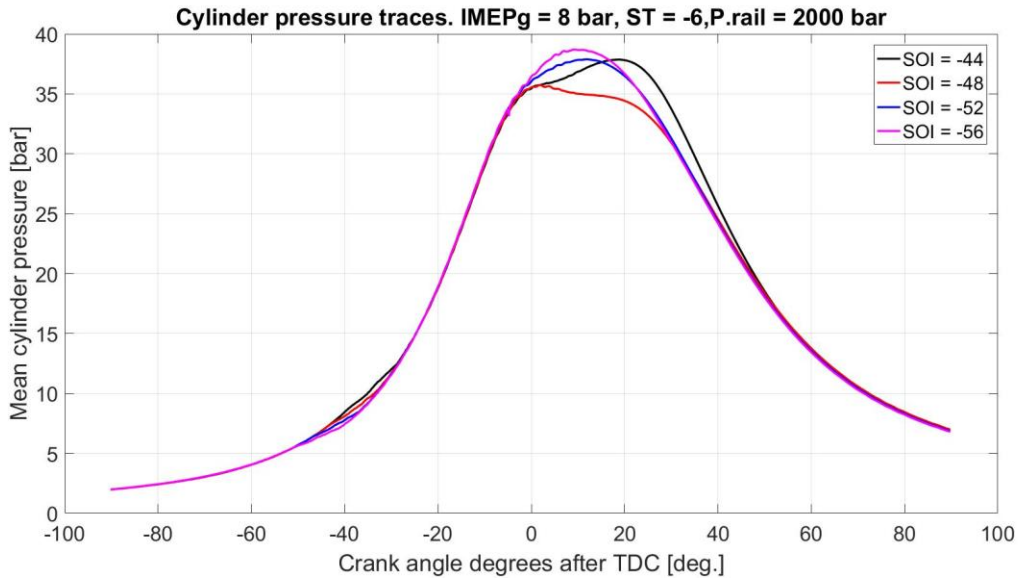

Figure 16 Mean cylinder pressures; P_{rail} =2000 bar, $IMEP_g$ = 8 bar, ST = -6 CAD ATDC, SOI = -44 to -56 CAD ATDC

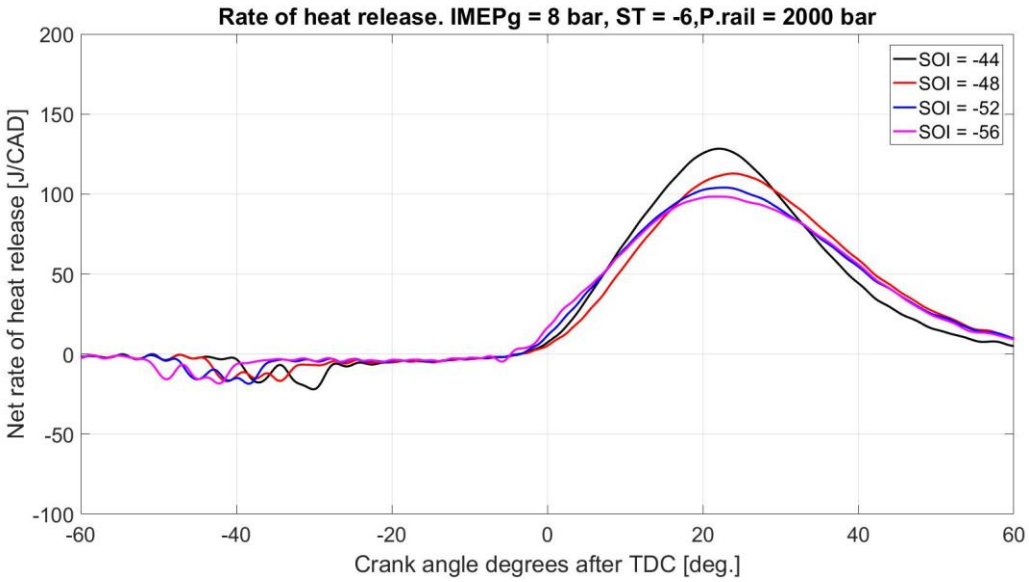

Figure 17 Heat release plots; P_{rail} =2000 bar, $IMEP_g$ = 8 bar, ST = -6 CAD ATDC, SOI = -30 to -40 CAD ATDC

Above in *Figure 16* and *Figure 17* are the mean cylinder pressure traces and respective heat release plots for the 'second group' of points at ST = -6. What is clear from the above plots is that neither the mean cylinder pressure nor the rate of heat release appear to show a combustion which would be associated with good efficiency. Due to the lack of a spike in the cylinder pressure traces and rate heat release plots. The explanation for this 'extra' group of points, compared to other operation sweeps, is that the high common rail pressure aided air entrainment into the fuel spray in combination with an earlier spark timing this enabled combustion to take place which although was not so efficient it did not vary significantly between cycles for the COV IMEPg to be above 10. Remembering that COV IMEPg under 10 was the requirement for what was considered stable combustion.

7.2.2 Common Rail Pressure 1500 bar

Parameter	Value
Common rail pressure	1500 bar
Engine Speed	1200 RPM
Lambda	1.5
Intake Temperature	85 ºC
Intake Pressure	1 bar
Exhaust Pressure	1 bar

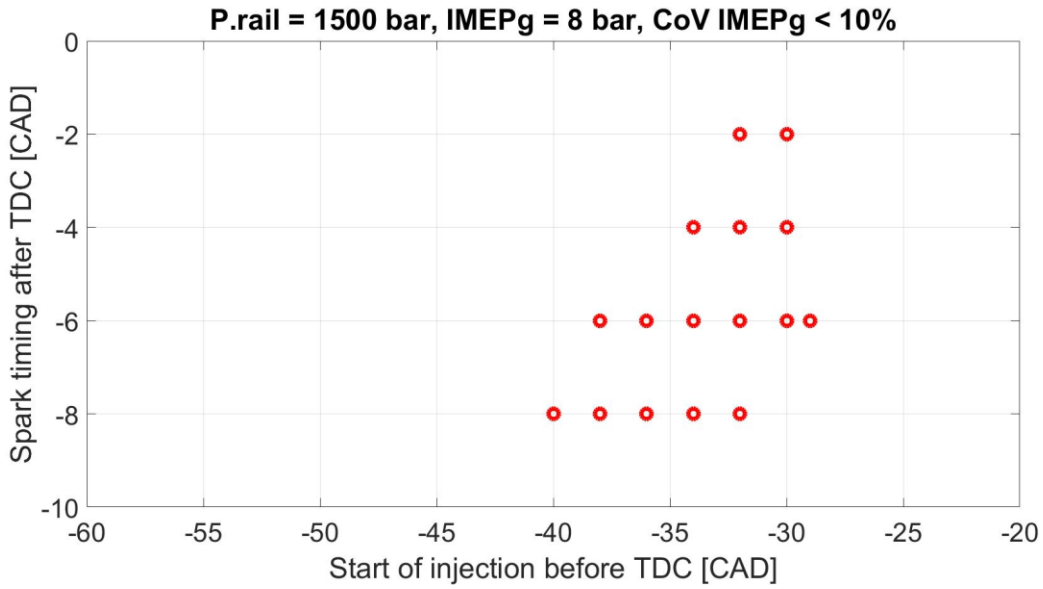

Figure 18 Operational points at 1500bar rail pressure

Operational sweep at a constant load of 8 bar IMEPg as before. Common rail pressure kept constant at 1500 bar. Start of injection swept from 40 to 29 CAD BTDC. Spark timing advance swept from -8 to -2 CAD BTDC. Each red ring indicates a point of stable combustion. The largest range of operational points was at ST = -6, in comparison to ST = -2 where only two operational points were fell within the criteria for stable combustion. The reason behind this is that at later spark timings is more likely to produce combustion abnormalities such as knock.

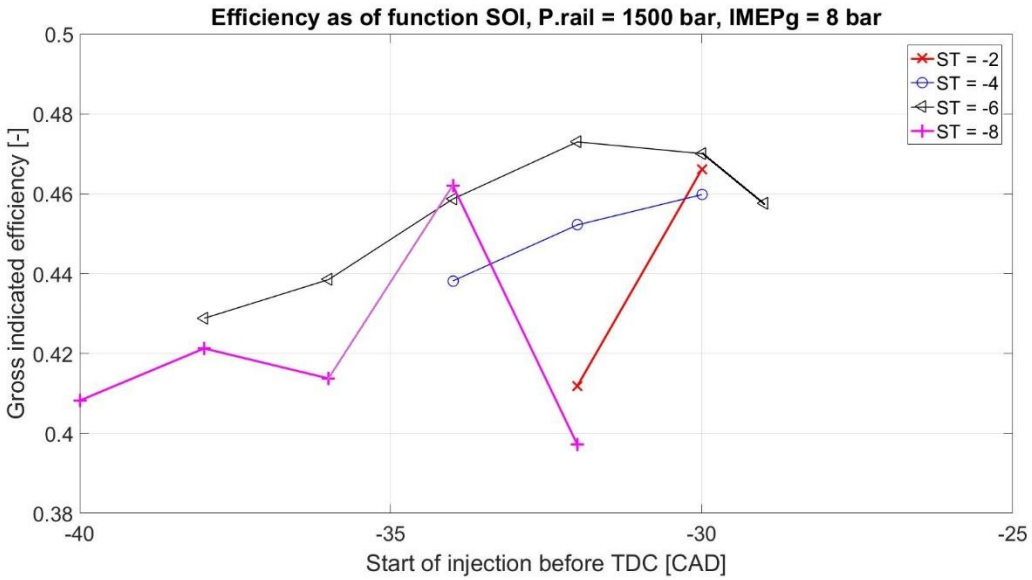

Figure 19 $\eta_{Gross\ Indicated}$; P_{rail} =1500 bar, $IMEP_g$ = 8 bar

Start of injection sweeps at ST = -2 and ST = -4 were knock limited, achieving only two data points at ST = -2 and three points at ST = -4. The lower common rail pressure appears to have reduced the operational range for these two spark timing sweeps. At 2000 bar rail pressure and ST = -2 (*Figure 8*) it was possible to achieve stable combustion in a range SOI = -31 to -23 CAD. Due to a lack of data points, optimal separation will not be calculated for ST = -2. SOI to ST optimal separation calculations for the remaining three sweeps all resulted in a separation of 26 CAD. The highest indicated efficiencies for these SOI sweeps ranged between 46 % and 47 %.

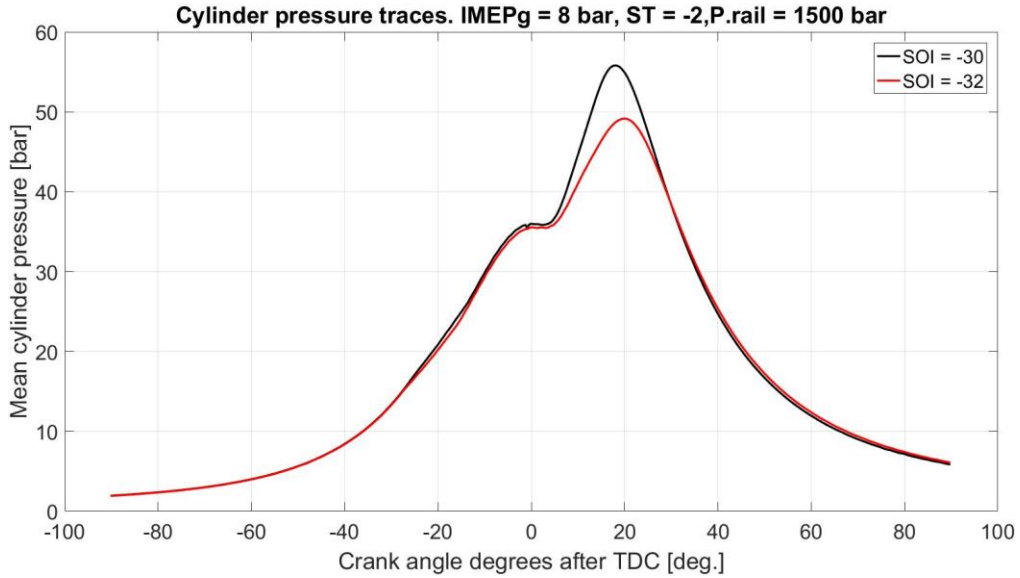

Figure 20 Mean cylinder pressures; P_{rail} =1500 bar, $IMEP_g$ = 8 bar, ST = -2 CAD ATDC

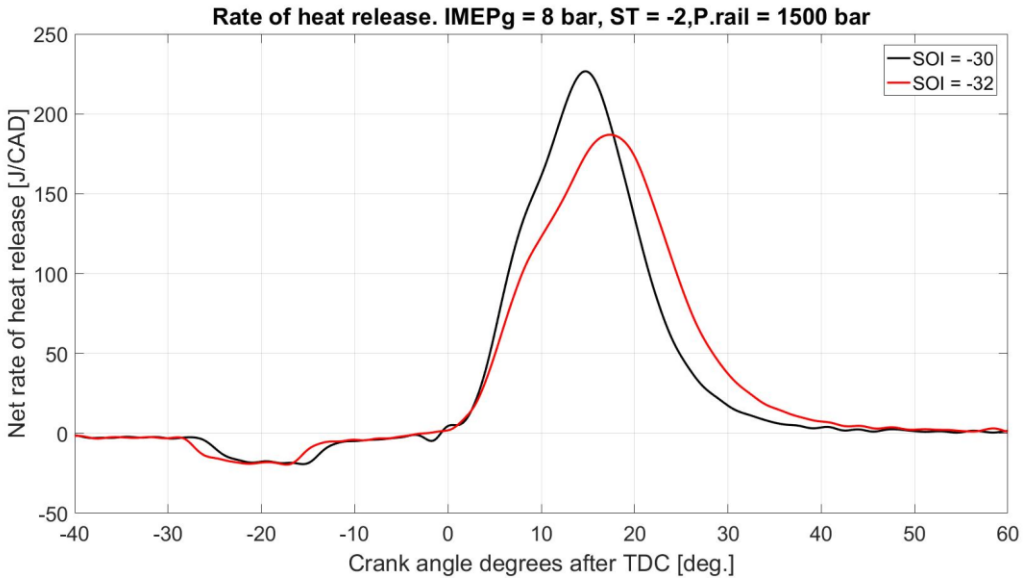

Figure 21 Heat release plots; P $_{rail}$ =1500 bar, IMEP$_g$ = 8 bar, ST = -2 CAD ATDC

Mean peak cylinder pressures at 48 and 56 bar combines with a narrow heat release peaking at 190 and 220 J/CAD respectively produce efficiencies of 41.2 and 46.6%. Comparison with the heat release plots for ST = -2 at 2000 bar pressure, where at SOI = -31CAD the base is also around 40 CAD and the peak is approx. 160 J/CAD, producing an efficiency of 45.4%. Very similar to results presented here. Concluding that reducing rail pressure has not had a noticeable effect on the combustion event itself.

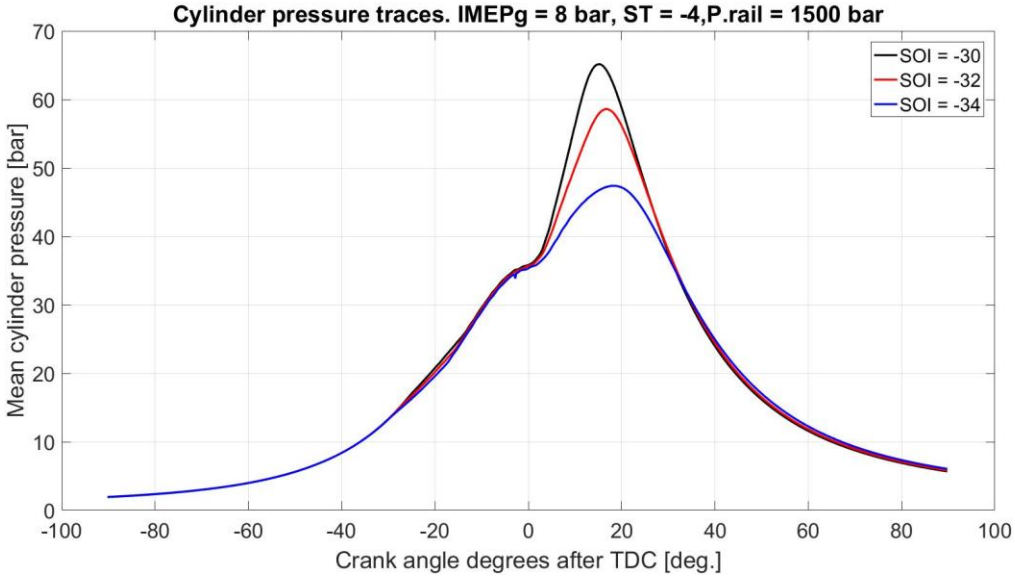

Figure 22 Mean cylinder pressures; P $_{rail}$ =1500 bar, IMEP$_g$ = 8 bar, ST = -4 CAD ATDC

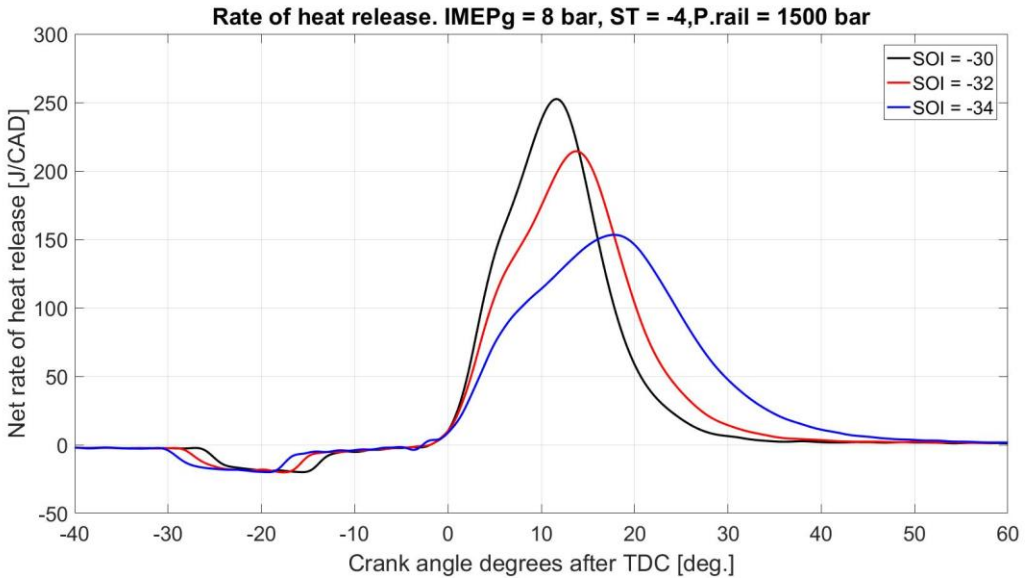

Figure 23 Heat release plots; P $_{rail}$ =1500 bar, IMEP$_g$ = 8 bar, ST = -4 CAD ATDC

Analysis of the mean cylinder pressure and heat release plots for start of injection sweeps at ST = -4 CAD again reveals the same trends and form. In comparison to results at higher rail pressures (2000 bar) it is concluded that the only noticeable effect in reducing rail pressure has been to reduce the operational range, as fewer injection timings were able to produce stable combustion at 1500 bar. Not only has the amount of points been reduced but also the injection timings are earlier.

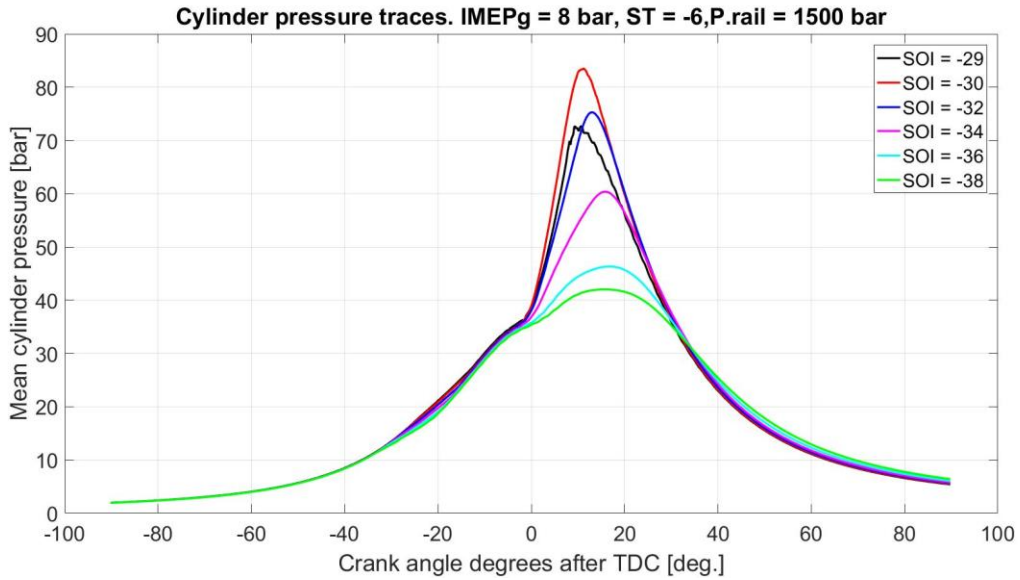

Figure 24 Mean cylinder pressures; P $_{rail}$ =1500 bar, IMEP$_g$ = 8 bar, ST = -6 CAD ATDC

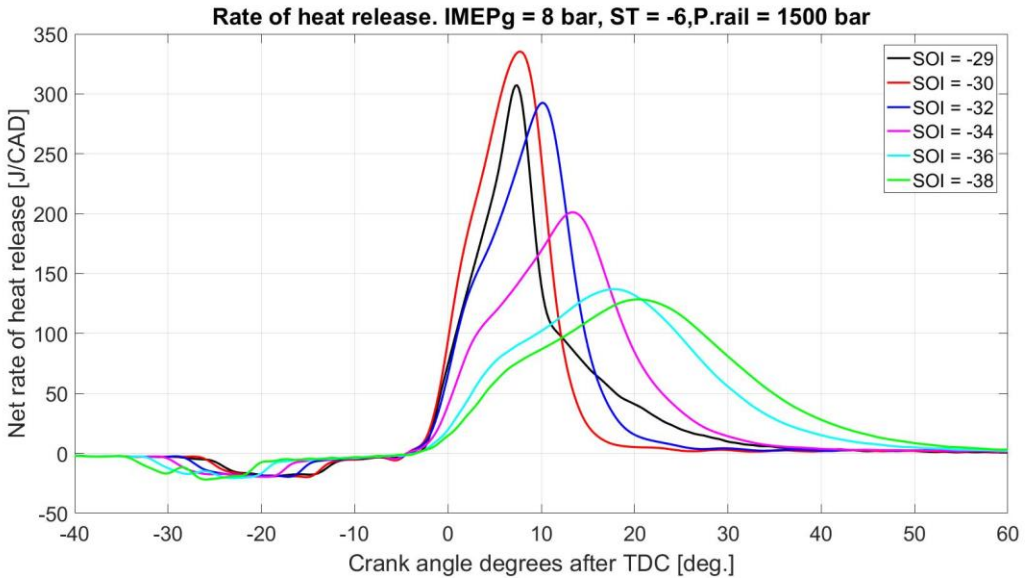

Figure 25 Heat release plots; P $_{rail}$ =1500 bar, IMEP$_g$ = 8 bar, ST = -6 CAD ATDC

The greatest amount of data has been collected at this spark timing for the operational sweep at rail pressure 1500 bar. In comparison to the results gained from the operational sweep where rail pressure was 2000 bar the range of injection timings is again decreased. Also consider the 'shoulder' which is apparent on the left side of the heat release curve. For example at SOI = -32 here in blue and at the same spark timing at P.rail = 2000 bar (*Figure 14 in red*) is apparently less pronounced here at P.rail = 1500 bar. However, the pronounced 'shoulder' could be a consequence of the scale on the Y-axis and therefore the piston bowl shape theory is not considered to be weakened by this observation.

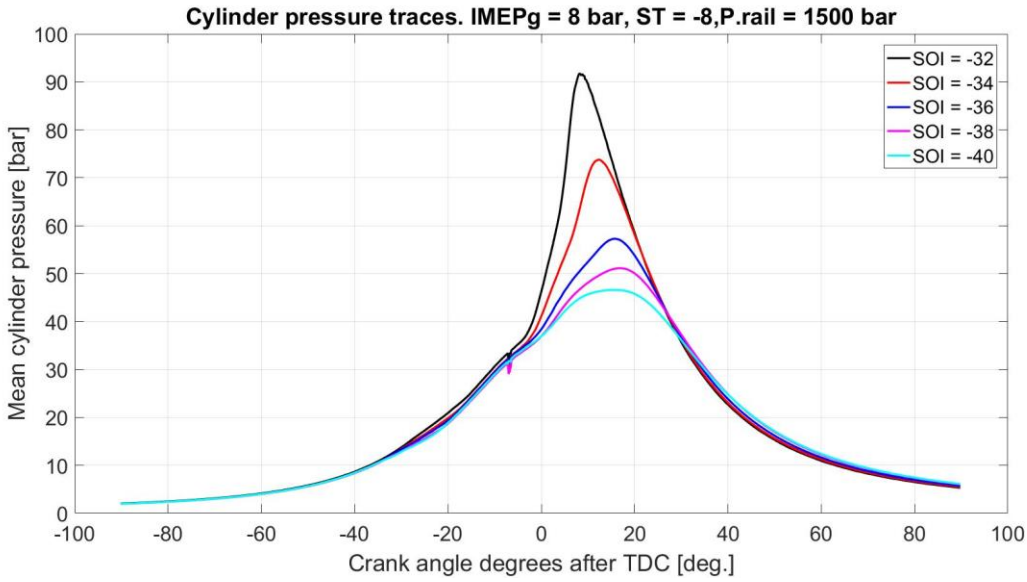

Figure 26 Mean cylinder pressures; P $_{rail}$ =1500 bar, IMEP$_g$ = 8 bar, ST = -8 CAD ATDC

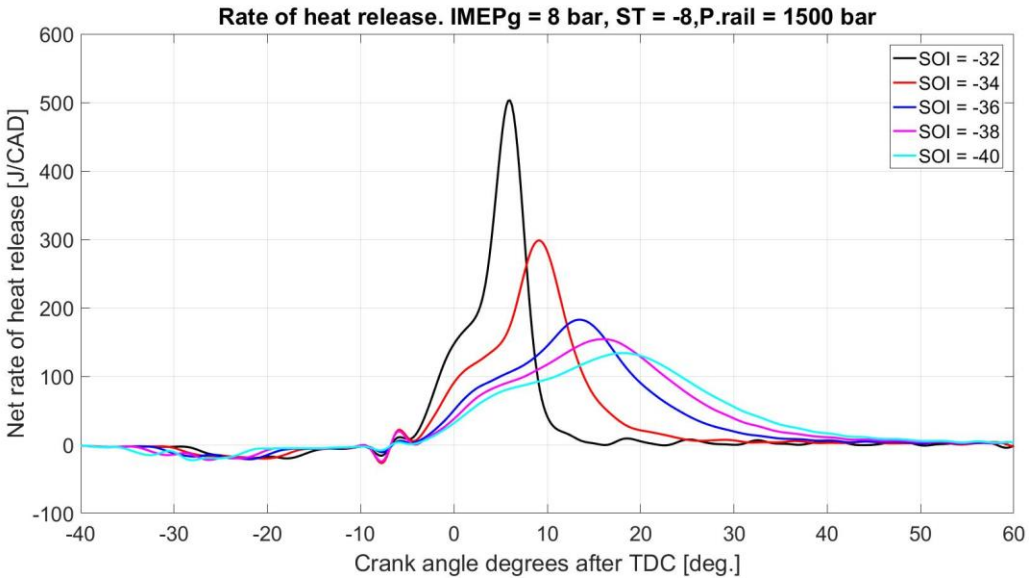

Figure 27 Heat release plots; P $_{rail}$ =1500 bar, IMEP$_g$ = 8 bar, ST = -8 CAD ATDC

Comparing the recorded efficiencies with the above plots, SOI = -32 (black line) $\eta_{\text{gross indicated}}$ = 39.7%, SOI = -34 (red line) $\eta_{\text{gross indicated}}$ = 46.2%, and SOI = -36 (blue line) $\eta_{\text{gross indicated}}$ = 41.4%. The highest efficiency therefore was not achieved from the highest mean peak cylinder pressure or highest peak rate of heat release. Again the conclusion for this is that the high rate of heat release seen at SOI = -32 CAD causes larger heat transfer losses. Again the 'shoulder' on the heat release here is once again more pronounced and the Y-axis scale is similar to that of *Figure 14.*

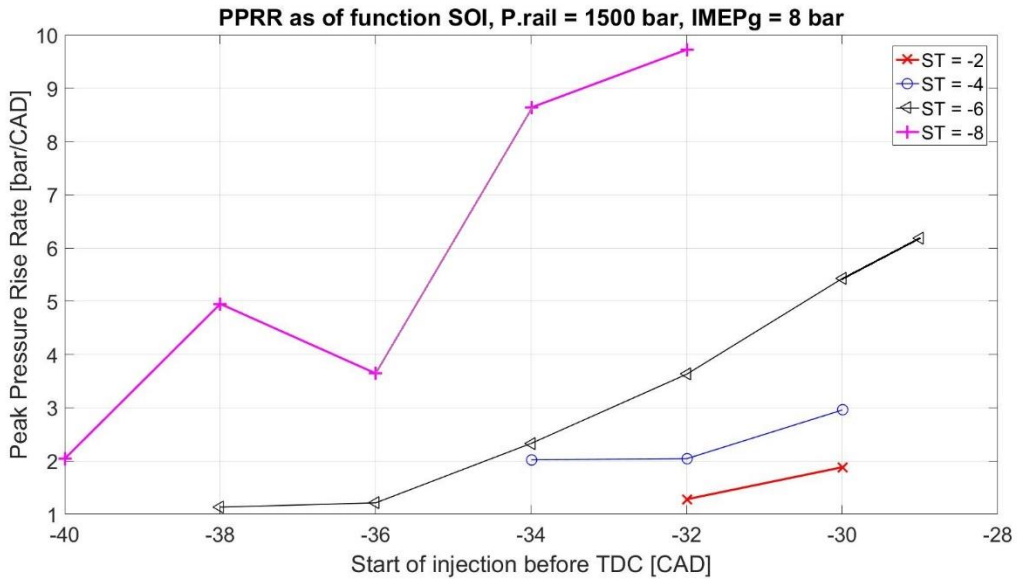

Figure 28 Peak Pressure Rise Rate P.rail = 1500 bar

Above in *Figure 28* the peak pressure rise rates for all of the operation points carried out at 1500 bar common rail pressure. The pressure rise rate is the gradient of the rate of heat release curve, where the highest value is then the PPRR. Here a correlation can be seen between the efficiency, rate of heat release and the PPRR. Which is best represented in a table where the SOI sweep at ST = -6 CAD ATDC is considered below *Table 4.*

Table 4

ST (CAD ATDC)	ST (CAD ATDC)	$\eta_{\text{Gross Indicated}}$ (%)	PPRR (bar/CAD)
-6	-29	45.8	6.18
-6	-30	47.0	5.43
-6	-32	47.3	3.63
-6	-34	45.9	2.33
-6	-36	43.9	1.22
-6	-38	42.9	1.13

The optimal PPRR is a trade-off, PPRR should be high enough so that the heat is released under a short time and therefore under less expansion, but not too high so that heat losses are too great.

7.2.3 Common Rail Pressure 1000 bar

Parameter	**Value**
Common rail pressure	1000 bar
Engine Speed	1200 RPM
Lambda	1.5
Intake Temperature	85 ºC
Intake Pressure	1 bar
Exhaust Pressure	1 bar

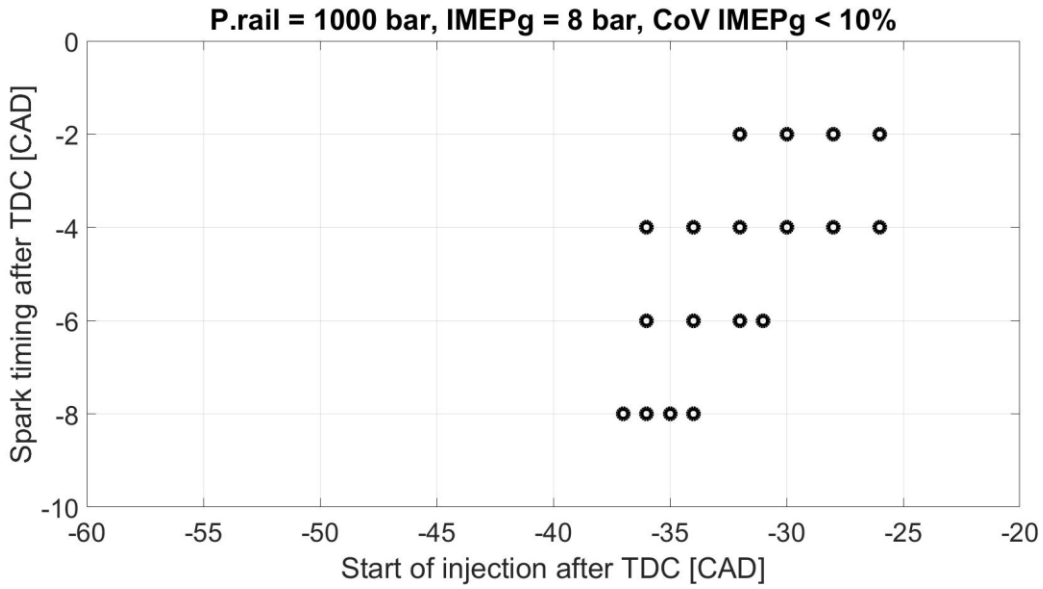

Figure 29 Operational points at 1000bar rail pressure

At this common rail pressure most data points collected and largest SOI range was on the ST = -4 sweep, the fewest data points and shortest SOI range was at ST = -8. The shape of the grouping of data points when compared with the operational sweep at rail pressure 1500 bar (*Figure 18*) appears almost inverted. Whereas the previous operational sweep, at 1500 bar common rail pressure, was knock limited at more retarded spark timings this operational sweep was limited at more advanced spark timings by cycle to cycle variation and poor combustion.

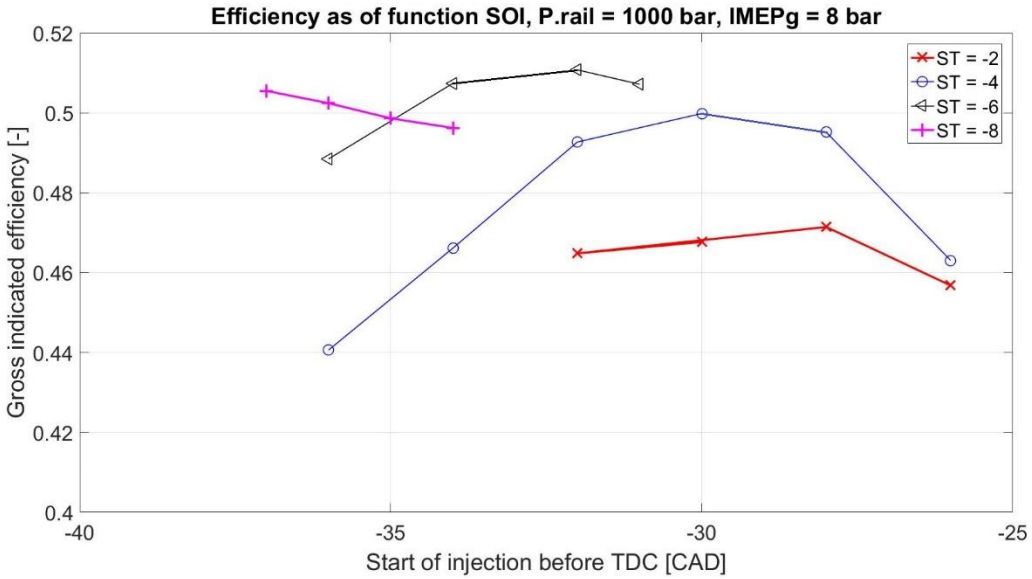

Figure 30 $\eta_{Gross\ Indicated}$; P_{rail} =1000 bar, $IMEP_g$ = 8 bar

Overall appearance of this chart is good, indicated efficiencies are generally higher than previous sweeps, three out of the four sweeps have a clear curve. These curves confirm hypothesis number one, that there is an optimal separation between SOI and ST. For the sweeps ST = -2, -4, -6 the optimal separation is 26 CAD.

In *Figure 31* below are mean cylinder pressure traces and heat release plots for SOI sweeps at ST = -4 and -6. Also a *Table 5* with corresponding combustion efficiencies and covariance of IMEPg. This is to further investigate the indicated efficiencies which are lower than would be expected when comparing peak cylinder pressures and heat release curves. These lower indicated efficiencies have previously been explained by increased heat transfer losses.

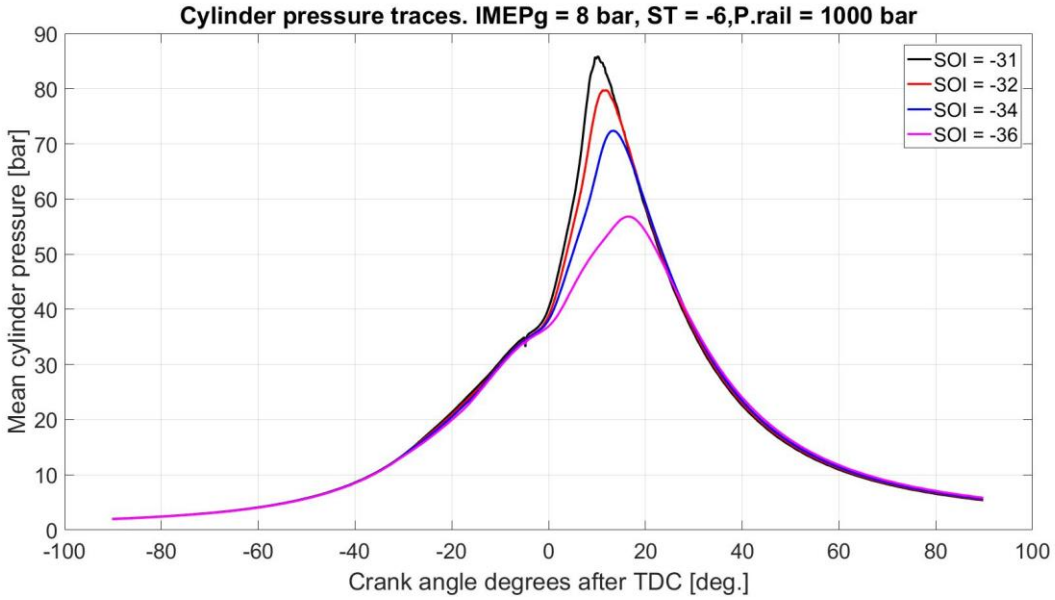

Figure 31 Mean cylinder pressures; P $_{rail}$ =1000 bar, IMEP$_g$ = 8 bar, ST = -6 CAD ATDC

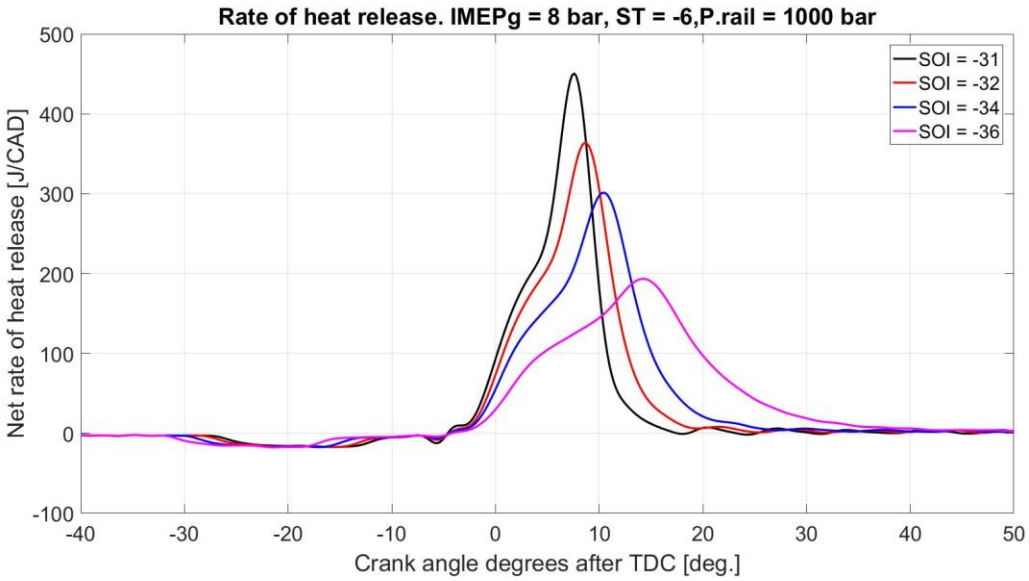

Figure 32 Heat release plots; P $_{rail}$ =1000 bar, IMEP$_g$ = 8 bar, ST = -6 CAD ATDC

Table 5 COV IMEPg and η $_{combustion}$; P $_{rail}$ =1000 bar, IMEP$_g$ = 8 bar, ST = -6 CAD ATDC

Start of injection (CAD after TDC)	Coefficient of variance for IMEPg(%)	Efficiency of combustion (%)
-31	2.29	99.69
-32	0.69	99.55
-34	0.84	99.16
-36	1.52	98.80

The highest indicated efficiency in this sweep was recorded at SOI = -32 although the combustion efficiency is lower than SOI = -31. COV IMEPg is higher for SOI = -31 than SOI

= -32 but this is not considered the reason for the lower indicated efficiency as the difference in combustion efficiency is considered negligible.

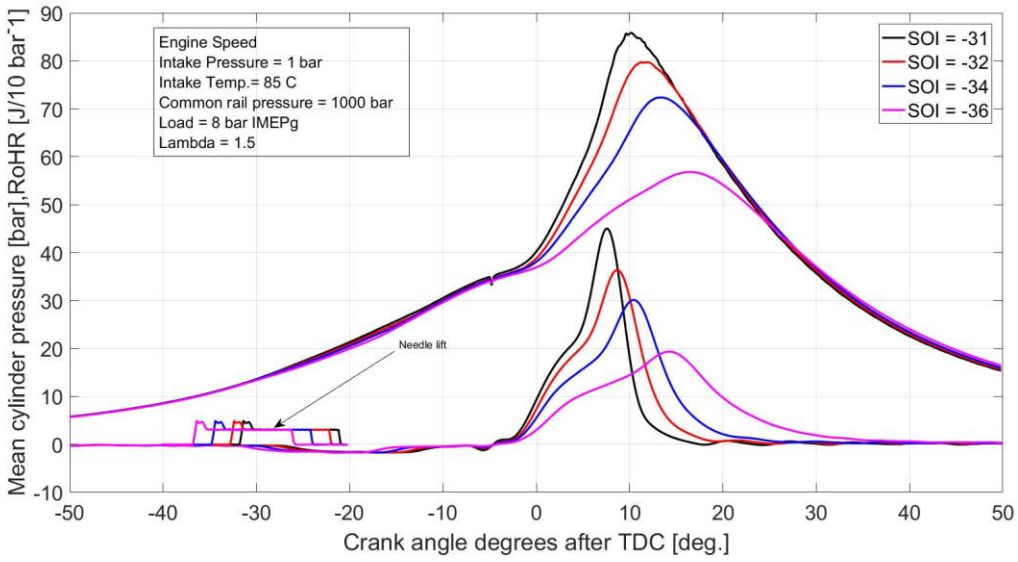

Figure 33 Cylinder pressure, heat release and needle lift.

In *Figure 35* above cylinder pressure, heat release and needle lift if plotted on the same chart. It is now possible to discern the relationship between fuel injection, fuel evaporation, and heat released during combustion. Clearly showing that the combustion is that of flame propagation and not a diffusion flame as in conventional diesel. Also apparent is the high sensitivity of this combustion concept.

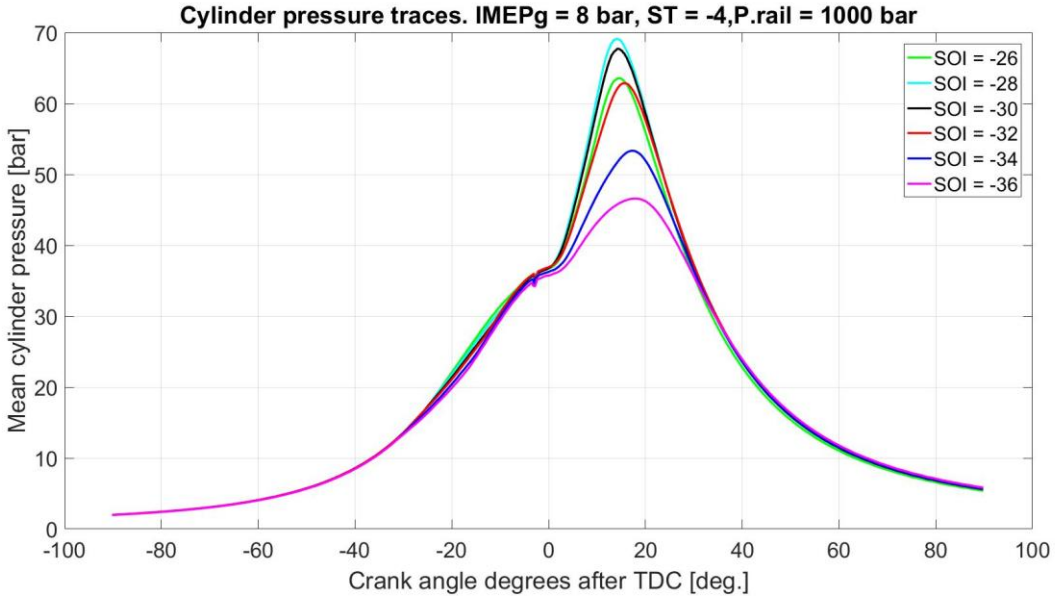

Figure 34 Mean cylinder pressures; P_{rail} =1000 bar, $IMEP_g$ = 8 bar, ST = -6 CAD ATDC

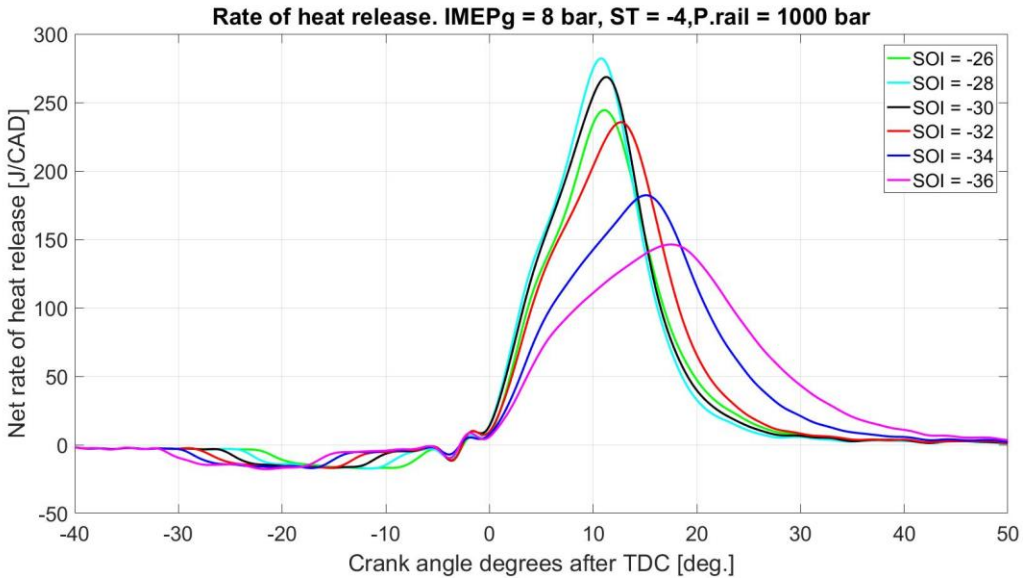

Figure 35 Heat release plots; P_{rail} =1000 bar, $IMEP_g$ = 8 bar, ST = -4 CAD ATDC

During this sweep at ST = -4 there was a problem with misfire, for that reason two different calculations for COV IMEPg were done. One where all 300 cycles were used including the cycles with misfire, and another where the cycles with misfire were not used to calculate COV IMEPg. The reason for the misfire is suspected to be carbon deposits on the spark plug that were remaining from another experiment.

Table 6 COV IMEPg and $\eta_{combustion}$; P_{rail} =1000 bar, $IMEP_g$ = 8 bar, ST = -4 CAD ATDC

Start of injection (CAD after TDC)	Coefficient of variance for IMEPg(%)	Efficiency of combustion (%)	Number of unfired cycles	COV IMEPg (%)
-26	3.37*	97.42	20	29.68
-28	0.23*	98.92	5	13.99
-30	1.01*	99.06	4	12.57
-32	1.11*	98.50	10	18.88
-34	2.35*	97.72	17	24.63
-36	4.26*	96.68	20	31.74

* cycles with no combustion have not been counted.

At this SOI sweep, spark timing was kept constant at ST = -4 CAD ATDC and the highest efficiency achieved at SOI = -30 CAD ATDC. At first glance the mean cylinder pressure traces and rate of heat release plots would suggest that SOI = -28 CAD should have the highest efficiency. Comparing the extra information from the above *Table 6* SOI = -30 and SOI = -28 have very similar combustion efficiency and lowest COV IMEPg is from SOI = -28. This confirms the conclusion that elevated heat transfer losses are the reason behind the lower efficiency for SOI = -28.

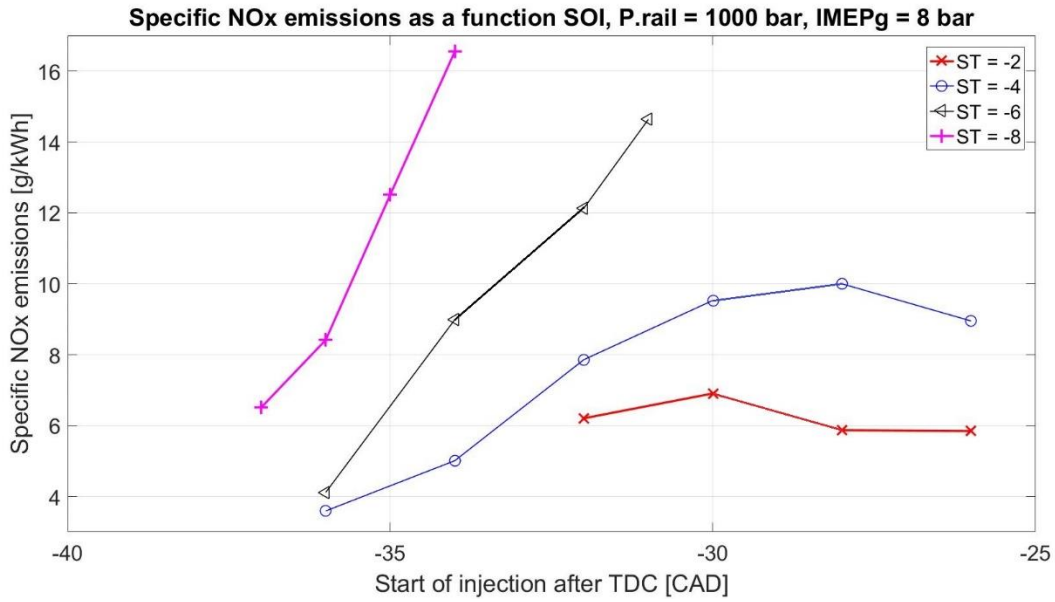

Figure 36 Specific NOx emissions; P. rail = 1000 bar, IMEPg = 8 bar.

No trends are apparent for specific NOx emissions and SOI or ST sweeps. The lowest emissions were around 4 g/kWh. Which are ten times higher than EURO VI emissions standards [15].

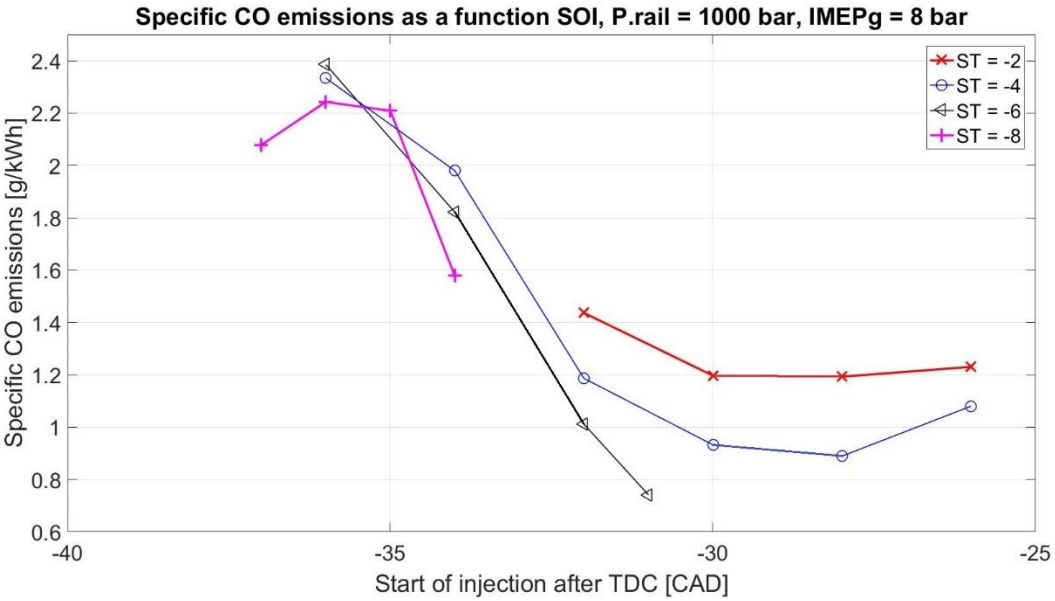

Figure 37 Specific CO emissions; P. rail = 1000 bar, IMEPg = 8 bar.

Specific CO emissions appear to decrease with retarded start of injection. The lowest recorded specific CO emission was 0.7 g/kwh. The EURO VI standard is 1.5 g/kWh [15]. Almost half of these results are below this standard and all results with a SOI equal to or later than -32 CAD ATDC were below the current European standard.

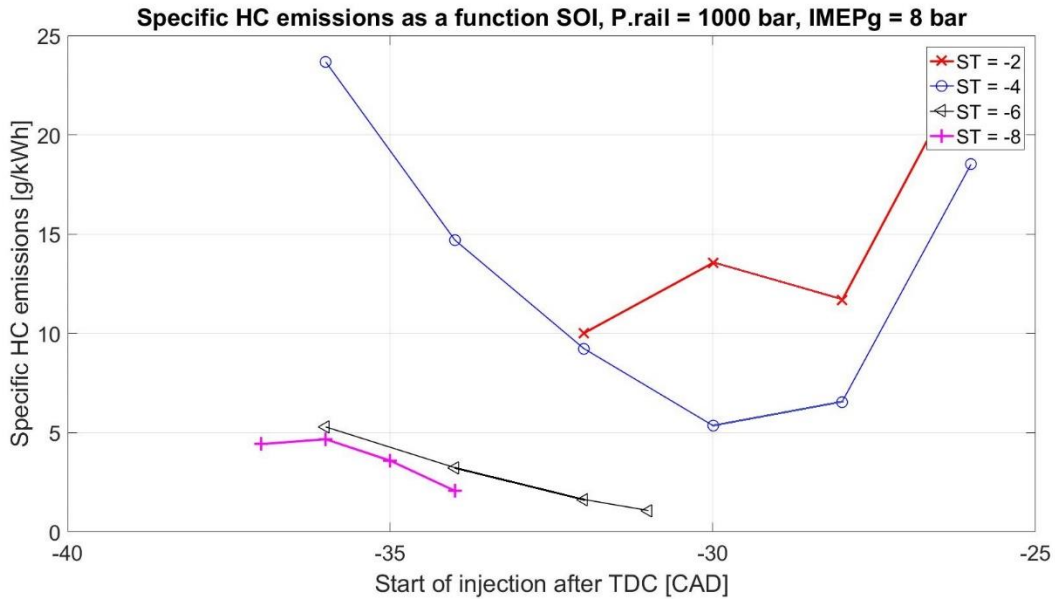

Figure 38 Specific HC emissions; P. rail = 1000 bar, IMEPg = 8 bar.

Specific HC emissions appear to decrease approaching SOI = -30 except for one data point at ST = -2 SOI = -30. The EURO emission standard is 0.13 g/kWh [15]. All recorded results exceeded this value. It is relevant to mention here that emission standards include engine and after treatment systems. This investigation measured only engine out emissions which explains the poor performance with regard to emission standards.

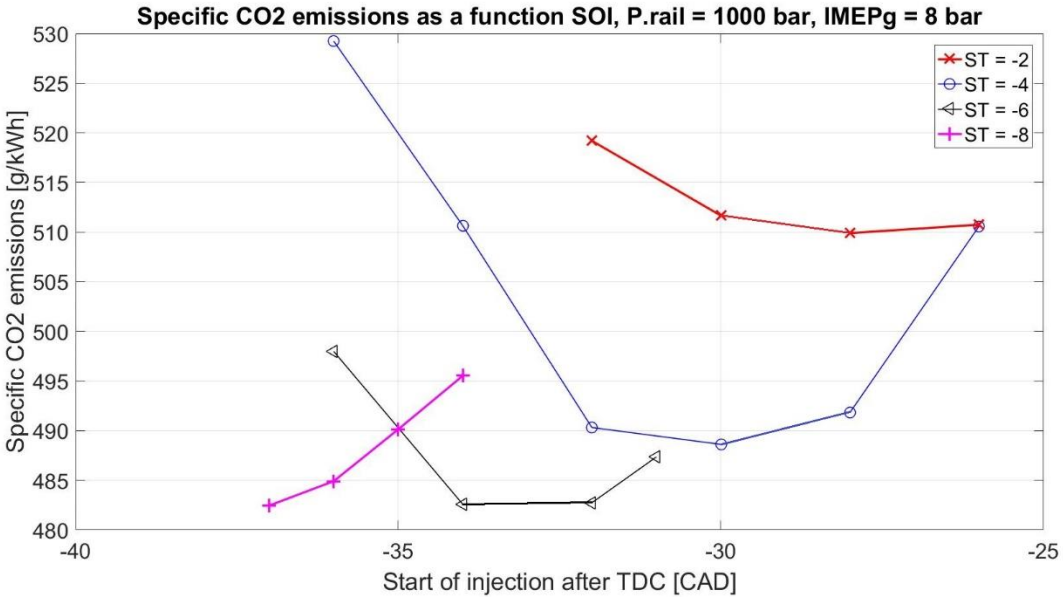

Figure 39 Specific CO2 emissions; P. rail = 1000 bar, IMEPg = 8 bar.

Specific CO_2 emissions are currently unregulated in Europe. No trends are apparent. That being said the specific CO_2 emissions are linked to combustion efficiency, CO and HC emissions.

7.3 EGR Sweep Constant Spark Timing

Investigation into the effect of EGR on load, lambda, combustion efficiency and emissions.

Parameter	Value
Common rail pressure	1500 bar
Engine Speed	1200 RPM
Start of Injection	-32 CAD ATDC
Intake Temperature	85 ºC
Intake Pressure	1 bar
Injection Duration	1390 µs
Spark Timing	-3 CAD ATDC

Since the intake pressure remained constant and the amount EGR is varied this meant that lambda values changed accordingly. The main purpose of this investigation was to see how this combustion concept reacted to EGR. For that reason, many parameters were held constant and the only variable was the amount of EGR.

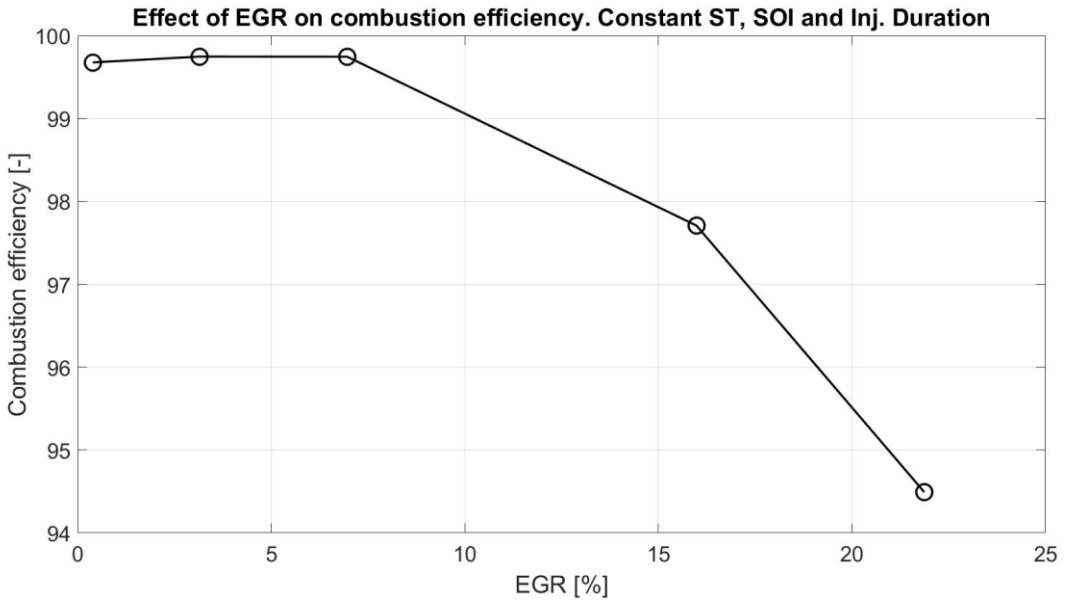

Figure 40 EGR and combustion efficiency, fixed spark timing..

As would be expected at higher amounts of dilution with EGR the combustion efficiency decreases. Methanol, according to previous studies is relatively resistant to EGR dilution. In *Figure 40* a combustion efficiency of over 97% can be observed with an EGR dilution of 15%. This would be considered normal for PFI SI but as has previously been show in this report 97% combustion efficiency is relatively poor.

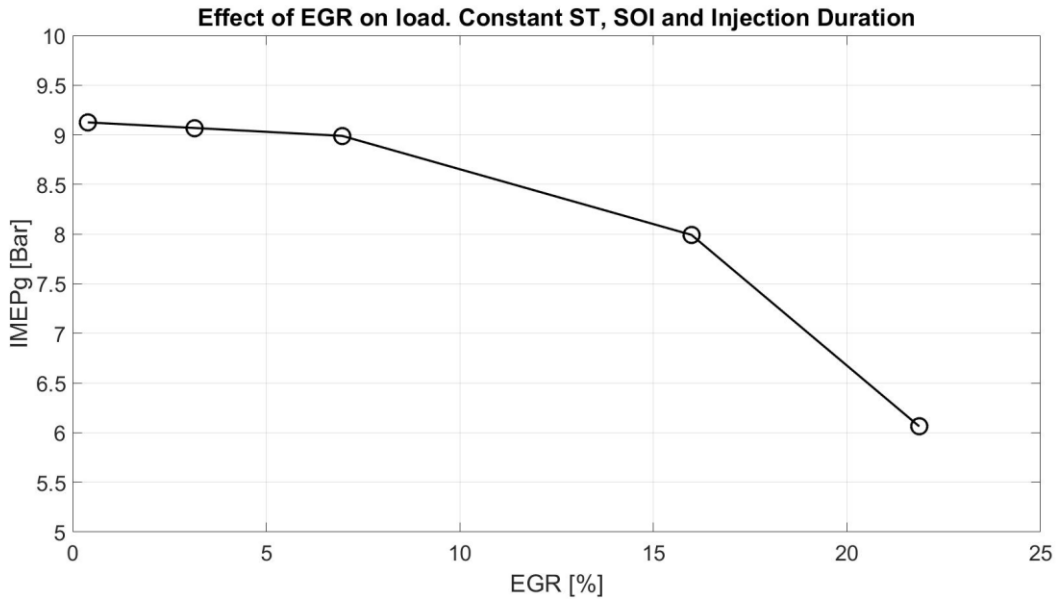

Figure 41 EGR and load, fixed spark timing.

The chart above (*Figure 41*) only reflects a drop in load due to a drop in combustion efficiency as shown in (*Figure 40*) The drop in load seems to be significantly more than would be explained by the reduction in combustion efficiency.

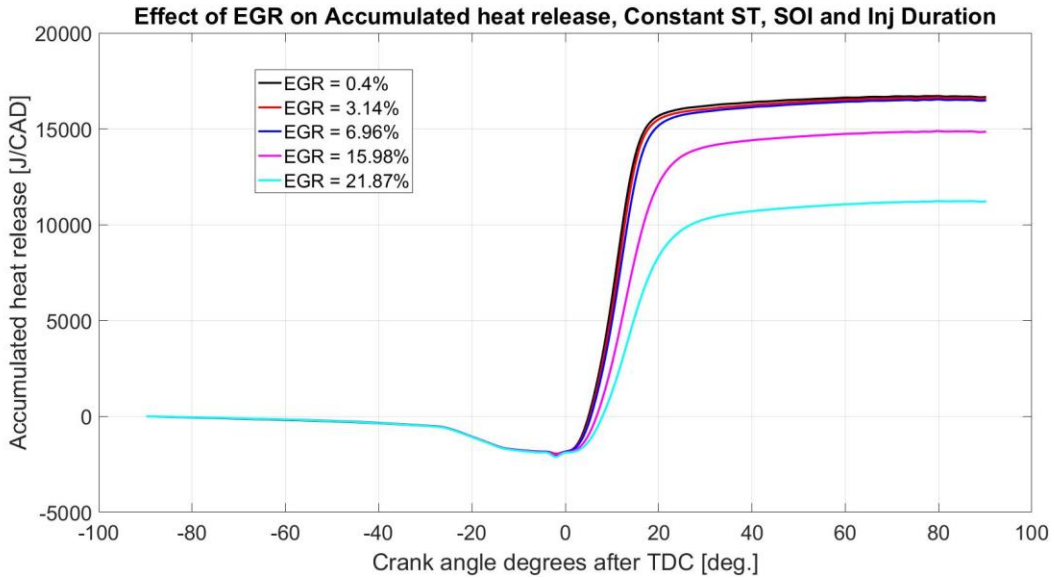

Figure 42 Effect of increased EGR on accumulated heat release. Fixed spark timing

A look at the accumulated heat release (*Figure 42*) shows that as EGR increases that total energy released from combustion is significantly reduced. This shows a maximum difference in total energy released from 0.4% EGR to 21.87% EGR as 16665 J – 11223 J = 5442 J (32.6%). However, it is clear from the combustion efficiency chart that the drop in combustion efficiency is only 99.68% - 95.49% = 5.19%. The injection pressure and duration are constant therefore the same amount of energy has been injected into the cylinder. That leaves the question ‘why is there apparently less energy released for higher EGR levels?’. The answer could be related to increased levels of EGR. It is suggested that the apparent difference in total energy released, in the accumulated heat release is down to elevated heating value of exhaust gases.

The *Table 7* below shows the crank angle which relates to the fraction of heat release for varied EGR levels. For example, the CA50 column shows the crank angle at which 50% of the total thermal energy has been released from the burning fuel. These values are calculated from the heat release data. It is clear that with increased EGR the combustion phasing is more delayed. Combustion duration is longer for increased EGR levels. EGR dilution is therefore inhibiting flame propagation. A longer combustion duration and later combustion phasing could lead to a loss of potential work as the combustion takes place during the expansion stroke. Longer combustion duration could also be expected to increase heat transfer losses to the piston and cylinder walls.

Table 7 Fraction of heat release for EGR sweep, fixed ST

EGR (%)	CA05 (CAD ATDC)	CA10 (CAD ATDC)	CA30 (CAD ATDC)	CA50 (CAD ATDC)	CA70 (CAD ATDC)	CA90 (CAD ATDC)	CA95 (CAD ATDC)
0.39	6	6.8	9.4	11.4	13.4	17.4	22
3.14	6.2	7	9.8	11.8	13.8	17.8	23.4
6.96	6.6	7.4	10.2	12.2	14.6	19	24.6
15.98	7.8	8.8	11.8	14.2	17.4	24	31.6
21.87	9	9.8	12.8	15.6	19	28	38.6

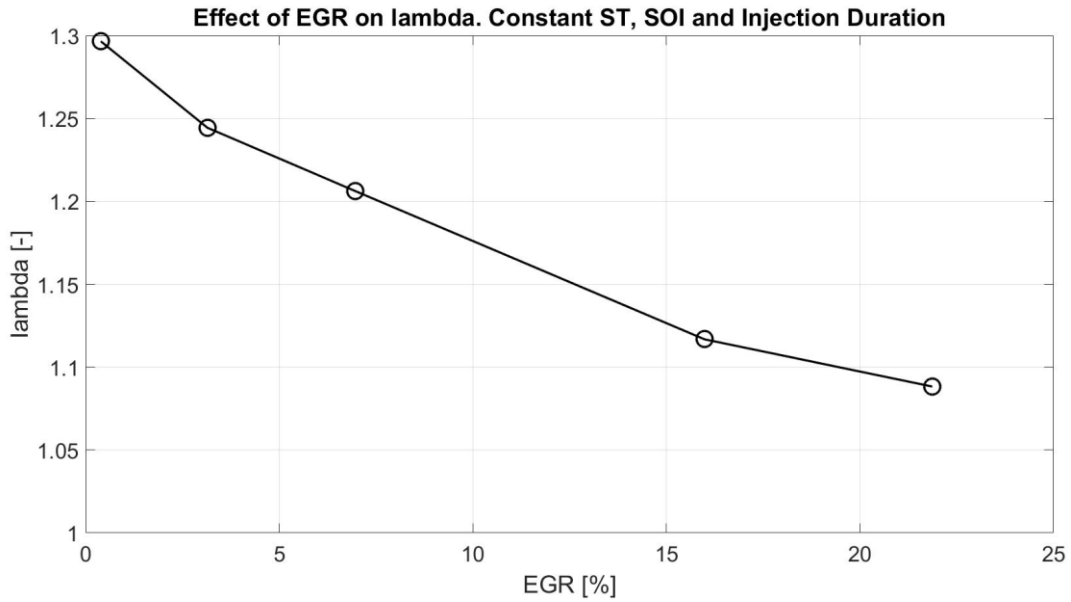

Figure 43 EGR and lambda, fixed spark timing.

In *Figure 43* increased EGR levels lead to decreased oxygen levels, the amount of fuel injected is kept constant and therefore this leads to a decreased lambda. Although the global fuel: air ratio is approaching unity towards the far right hand side of this chart, the fuel distribution in this combustion concept (DISI) is not homogenous and therefore benefits from a globally lean mixture, thus ensuring sufficient oxygen is present around the fuel spray and subsequent flame propagation area within the piston bowl.

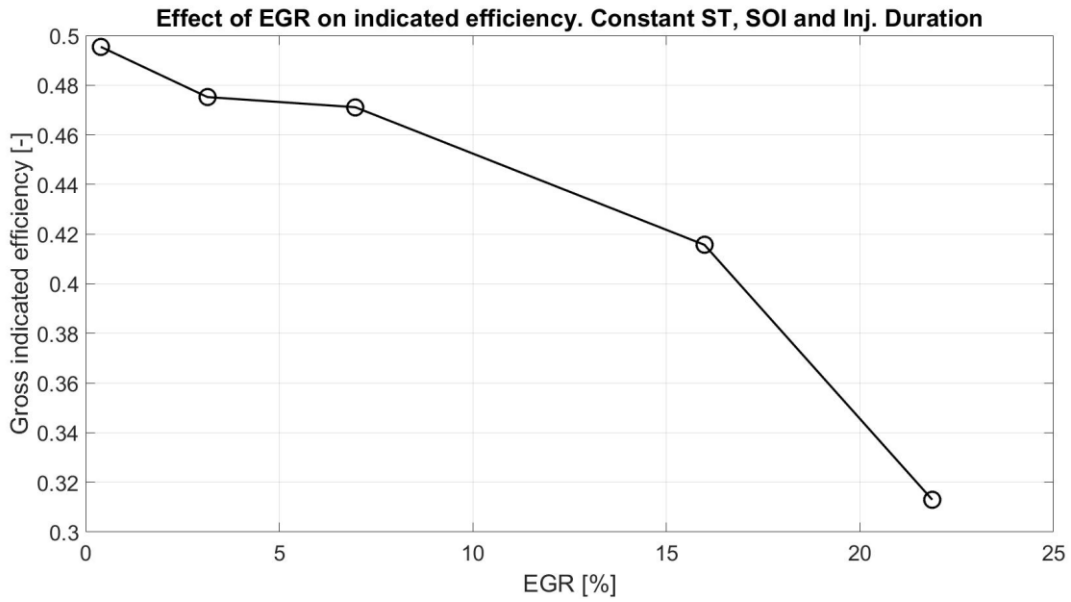

Figure 44 EGR and Indicated efficiency, fixed spark timing.

In the above *Figure 44*, decrease in indicated efficiency is the result of decreased combustion efficiency, greater heat transfer losses and increased cooling effect caused by increasing EGR levels.

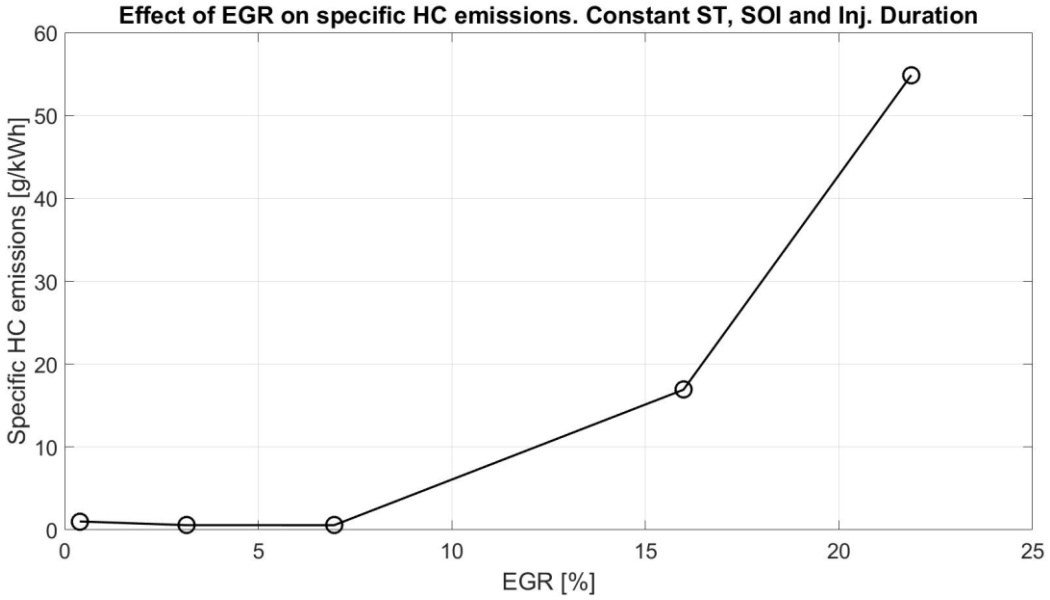

Figure 45 EGR and Specific HC emissions, fixed spark timing.

Looking at the specific hydrocarbon emissions, dilution with EGR lowers the oxygen content in the cylinder. Less oxygen would be expected to lead to increased HC and CO emissions, which confirms observations in *Figure 45* and *Figure 46*. Obviously with decreased combustion efficiency, increased unburned HC emissions would be expected.

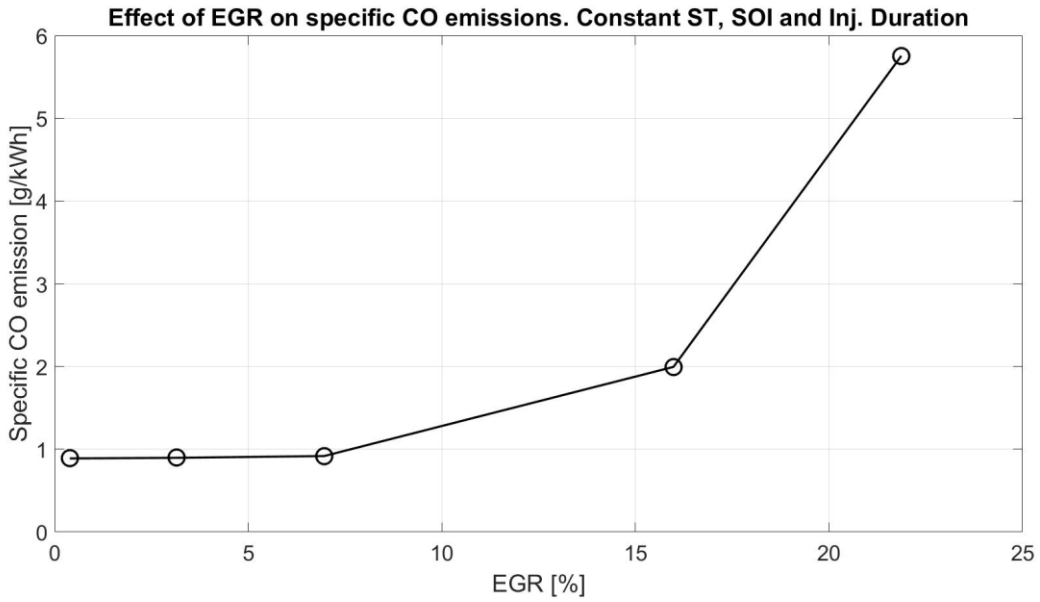

Figure 46 EGR and Specific CO emission, fixed spark timing.

In *Figure 46* increased EGR leads to increased specific CO emission, one reason for this has already been explained above, but this could also be due to EGR reducing combustion temperature because EGR has a higher specific heat value than the air it replaces. A reduction in combustion temperature could also inhibit further oxidation of CO to CO_2.

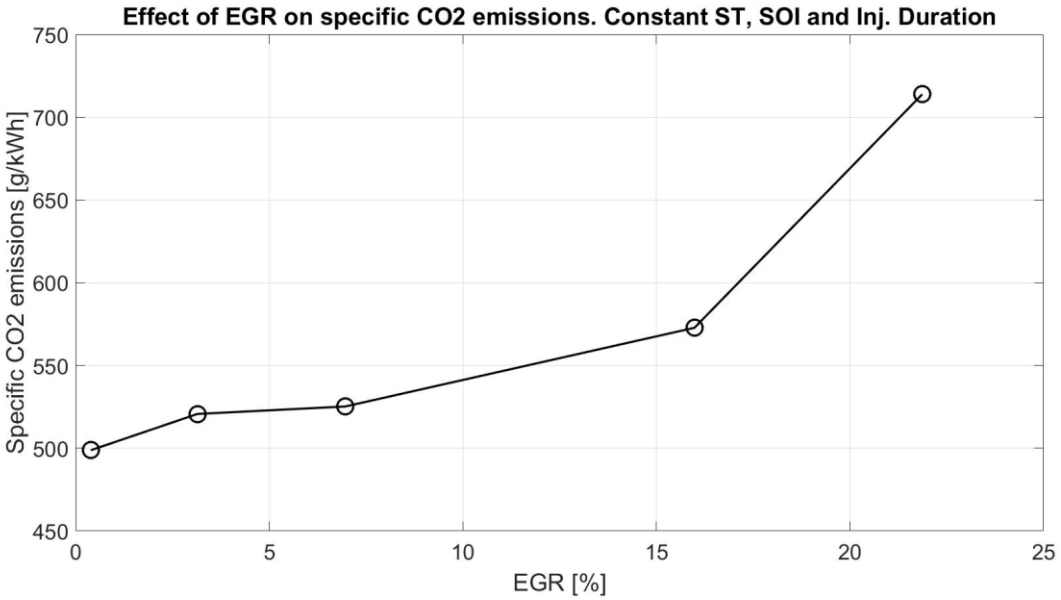

Figure 47 EGR and Specific CO_2 emissions, fixed spark timing.

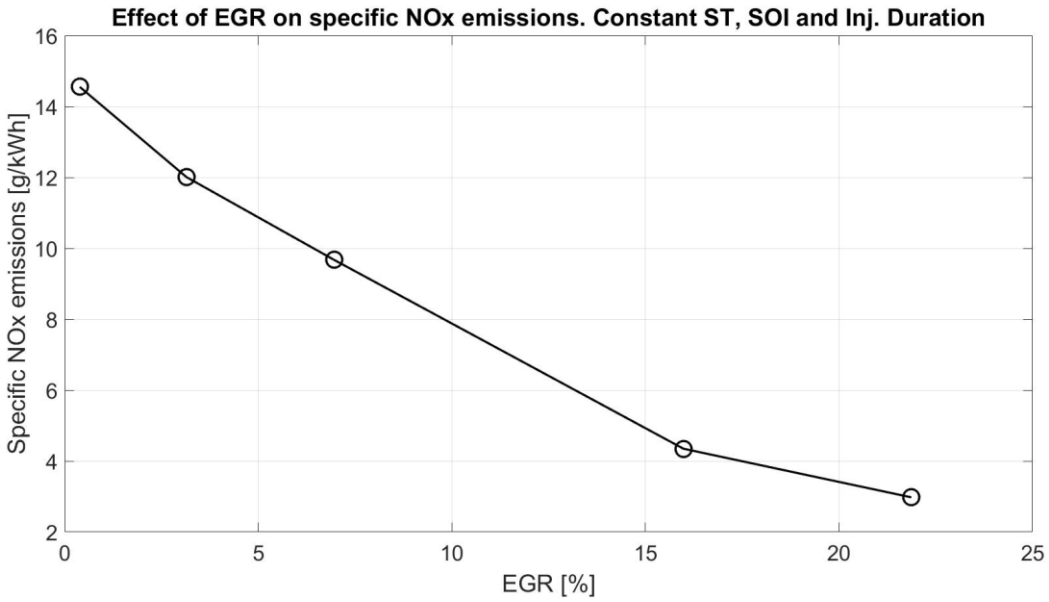

Figure 48 EGR and Specific NOx emissions, fixed spark timing.

NOx emissions are reduced by additional EGR. This confirms hypothesis three.

7.4 EGR Sweep Variable Spark Timing

Now that the overall effect of EGR has been investigated. The next section will try to answer the question: Can combustion efficiency be improved by adjusting the spark timing?

Parameter	Value
Common rail pressure	1500 bar
Engine Speed	1200 RPM
Start of Injection	-32 CAD ATDC
Intake Temperature	85 ºC
Intake Pressure	1 bar
Injection Duration	1390 μs

Again intake pressure is held constant, and EGR levels increased which will lead to a decrease in lambda. The same fuel injection pressure, timing and duration as the previous sweeps were used.

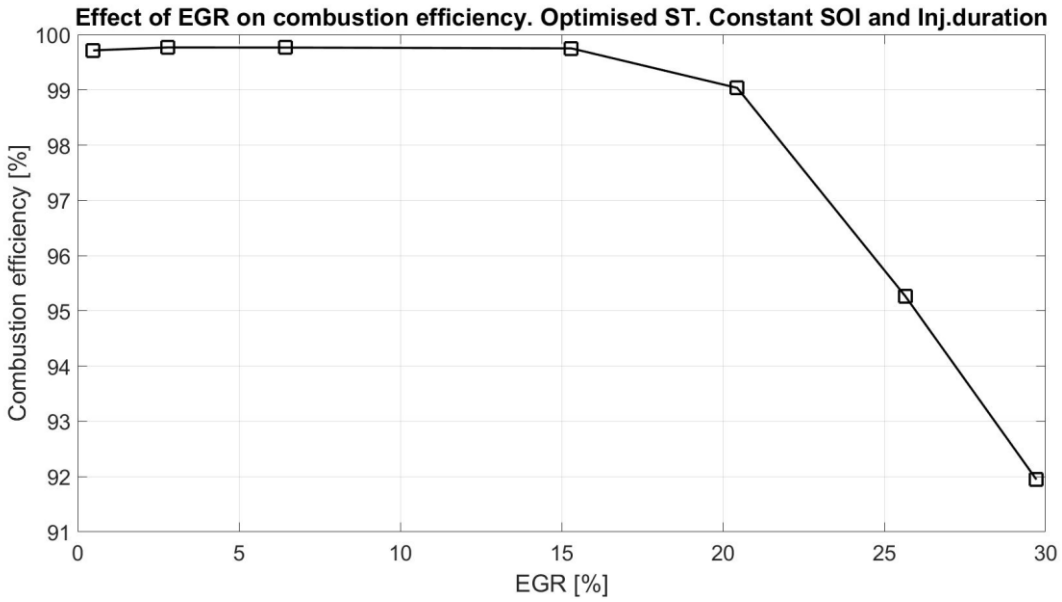

Figure 49 EGR and combustion efficiency, variable spark timing.

As seen in *Figure 49* combustion efficiency is kept above 99% up to an EGR level of 20%. Compared with the fixed spark timing sweep where for the same EGR level combustion efficiency was below 95%, this is a huge improvement.

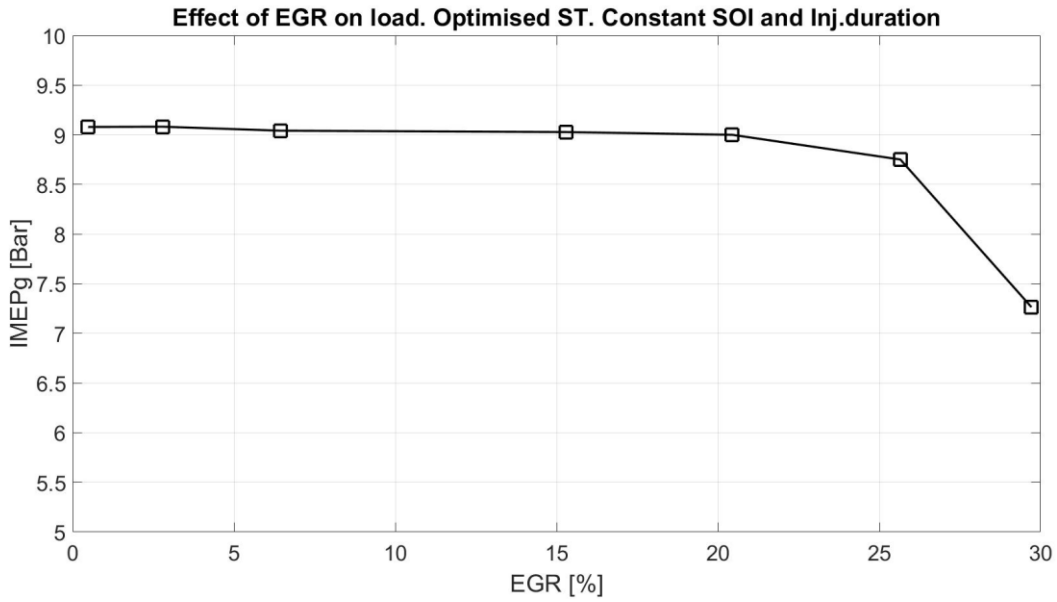

Figure 50 EGR and load, variable spark timing.

Load was subsequently held constant at 9 bar IMEPg well up to 20% EGR.

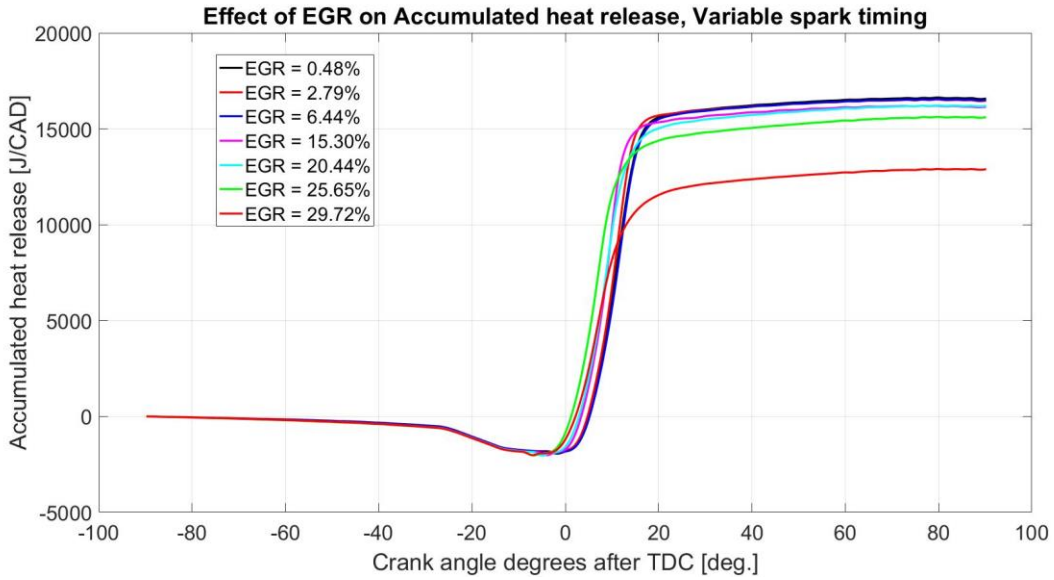

Figure 51 Accumulated heat release for variable spark timing.

Above in *Figure 51* it is observed that a greater cumulative total amount of energy has be observed on all but the highest EGR concentration. This would then strengthen the argument in the last section that potential work was being lost due to an increased combustion duration during the expansion stroke. This theory is support by the data in *Table 8* which, if CA50 values are compared, shows that combustion phasing is place earlier and earlier for increased EGR levels. Also as before, combustion duration increases as EGR is increased. As seen in the previous EGR sweep with fixed spark timing, EGR inhibits flame propagation. However, when the spark timing can be advanced then combustion can be phased earlier, thus diminishing the loss of work caused by the cylinder volume expanding.

Table 8 Fraction of heat release for EGR sweep with variable ST

EGR (%)	ST (CAD ATDC)	CA05 (CAD ATDC)	CA10 (CAD ATDC)	CA30 (CAD ATDC)	CA50 (CAD ATDC)	CA70 (CAD ATDC)	CA90 (CAD ATDC)	CA95 (CAD ATDC)
0.48	-3	6	6.8	9.4	11.4	13.4	17	23
2.79	-3	5.8	6.6	9	11	12.6	15.4	20
6.44	-3	6.2	7	9.6	11.6	13.6	17.2	23
15.30	-5	4.4	5.2	7.6	9.4	10.8	14.2	21.4
20.44	-6	4	4.8	7.4	9.2	11.2	16.8	27.6
25.65	-8	2.2	3	5.4	7.4	9.4	16.8	31
29.72	-8	3.2	4	6.4	8.4	11.2	20.6	34.8

Indicated efficiency remains relatively constant around 46-47% up to EGR levels of 20%.

The corresponding spark timings can be seen in the *Table 9* below.

Table 9 EGR, SOI, ST, η gross indicated

EGR [%]	SOI [CAD ATDC]	ST [CAD ATDC]	$\eta_{\text{gross indicated}}$
0.48	-31	-3	0.47
2.79	-31	-3	0.48
6.44	-31	-3	0.46
15.30	-31	-5	0.47
20.44	-31	-6	0.47
25.65	-31	-8	0.46
29.72	-31	-8	0.38

The spark timing was optimised for highest efficiency *Table 9.* As discussed above the more advanced spark timing for greater levels of EGR, advances combustion phasing to optimise indicated efficiency. Advancing the spark timing has the effect of decreasing the optimal separation of 28 CAD at 0.48% EGR to a separation of 23 CAD at 25.6% EGR. The final point in the *Table 7* was not taken into account due to a lower indicated efficiency.

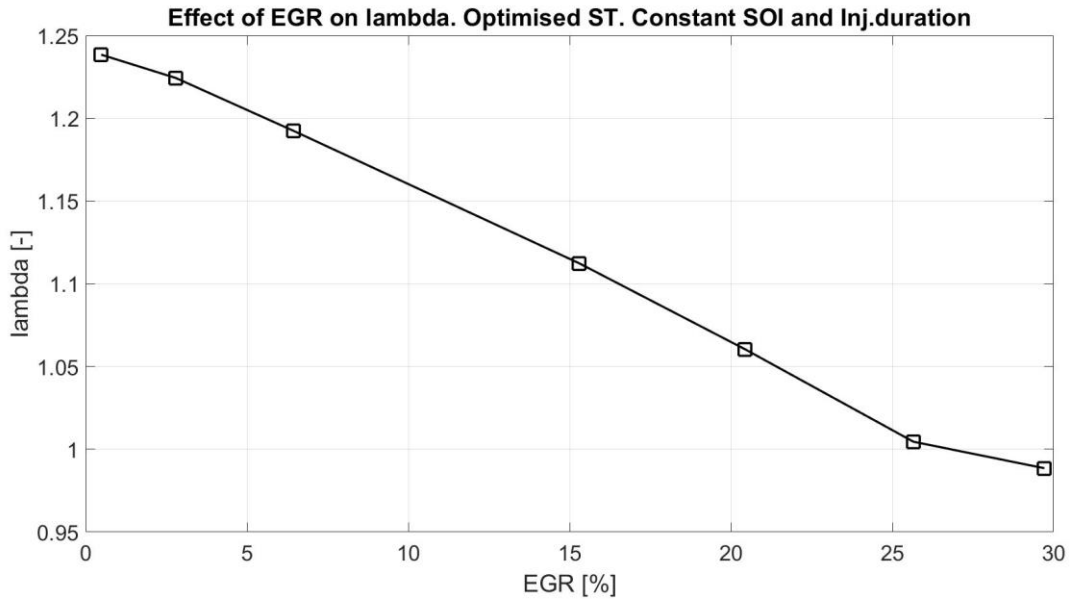

Figure 52 EGR and lambda, variable spark timing.

Lambda reduced linearly with EGR as would be expected, as air was being replaced with exhaust gases.

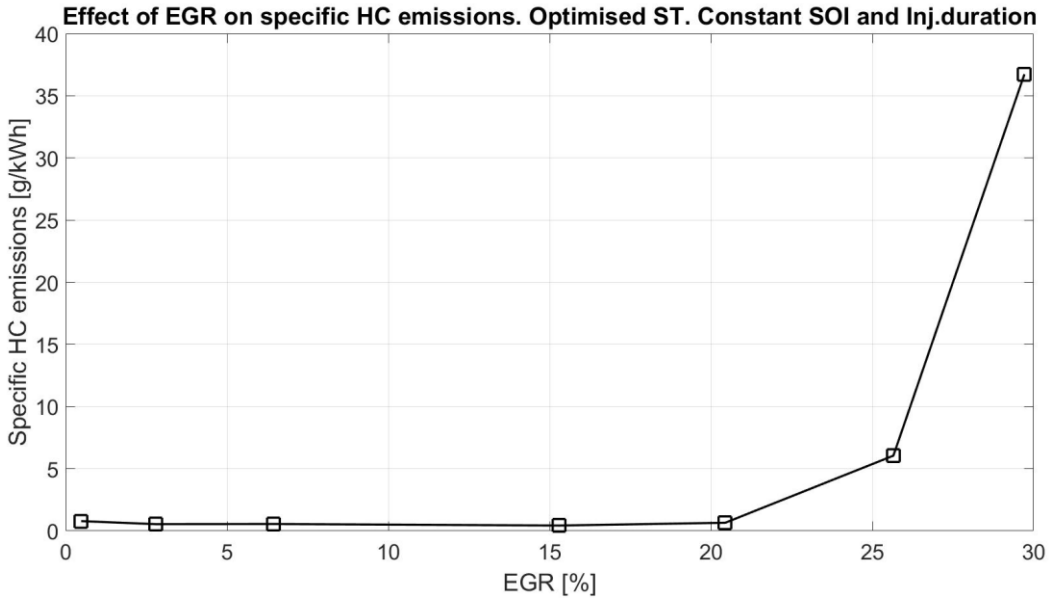

Figure 53 EGR and Specific HC emission, variable spark timing.

As expected by looking at the high combustion efficiency in *Figure 49* the HC emissions are constantly below 0.8g/kWh up to 20% EGR. The EURO VI emission standard is 0.13g/kWh. Combustion phasing is also more advanced as EGR levels increased, giving more time for the remaining oxygen in the cylinder to react with the fuel.

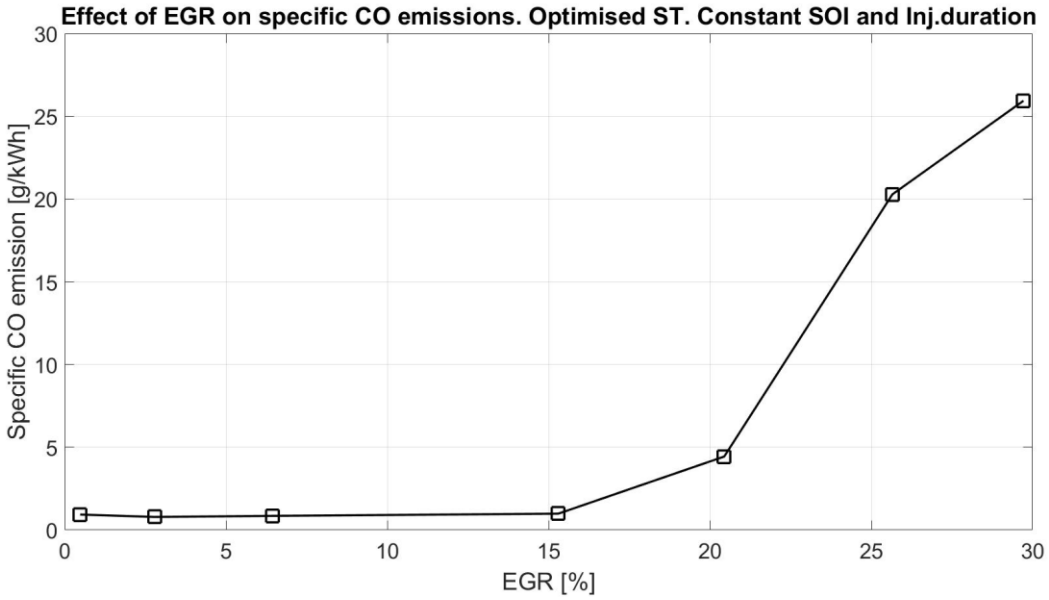

Figure 54 EGR and Specific CO emission, variable spark timing.

Specific CO emissions are held below 1g/kWh until 15% EGR when it begins to rise. The EURO VI emission standards set the limit at 1.5g/kWh. The rise in CO emission at EGR levels above 15% is likely due to the reduction in available oxygen.

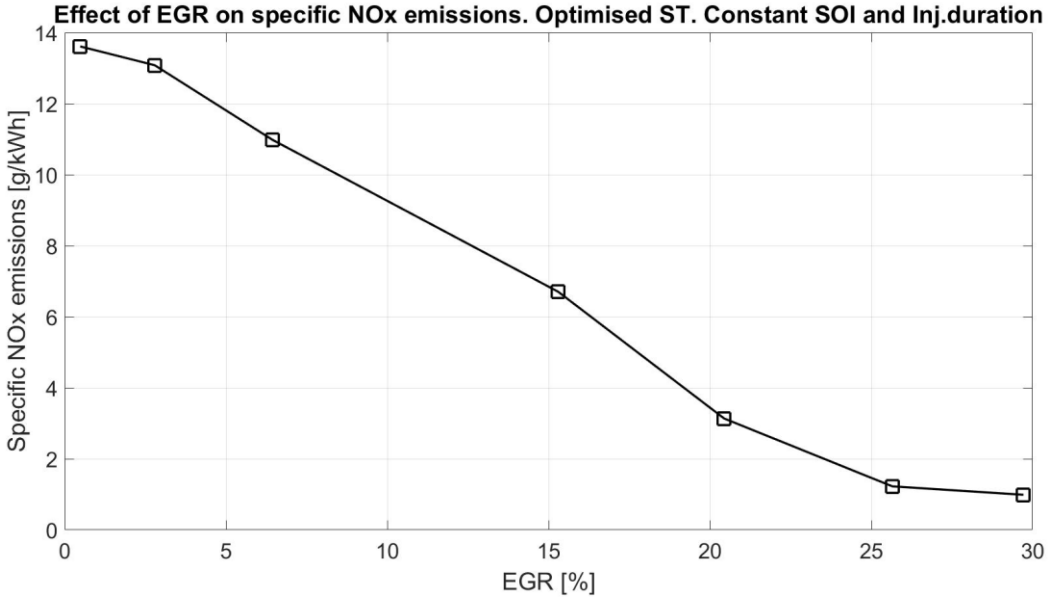

Figure 55 EGR and Specific NOx emission, variable spark timing.

A steady decrease in NOx emissions is observed as EGR levels are increased, but all levels are above the current EURO VI standard of 0.4 g/kWh.

Exhaust after treatment would then be a requirement for this combustion concept giving the results achieved here.

7.5 Future Research

Suggestions for future research would be to further investigate start of injection timings. Possibly very advanced fuel injections to allow for a more homogenous fuel air mixture at the time of ignition. Success in this is likely to be achieved at higher common rail pressures which would improve air entrainment. This would likely lead to increased crevices losses but could allow for a greater level of EGR to be added. Increased EGR and more boost could well improve overall efficiencies due to increased cooling effect which would lead to increased knock suppression. Combustion at stoichiometric fuel: air mixtures would also allow for effective use of a TWC exhaust after treatment system.

The position of the spark plug in relation to the fuel injector should be investigated. Moreover, investigation into the effect of spark plug orientation and electrode depth is advised.

A lower compression ratio could also be investigated; this would allow for greater spark timing optimisation due to less combustion abnormalities. According to Heywood the optimal compression ratio should be 15:1 [8].

Soot levels were not measure in this investigation as they were expected to be low, this should be confirmed by experimentation.

During the course of this investigation several points of high efficiency were discovered as seen in below *Figure 56*. Discovering the reasons for these high efficiencies is no doubt the key to advancing methanol DISI as a concept.

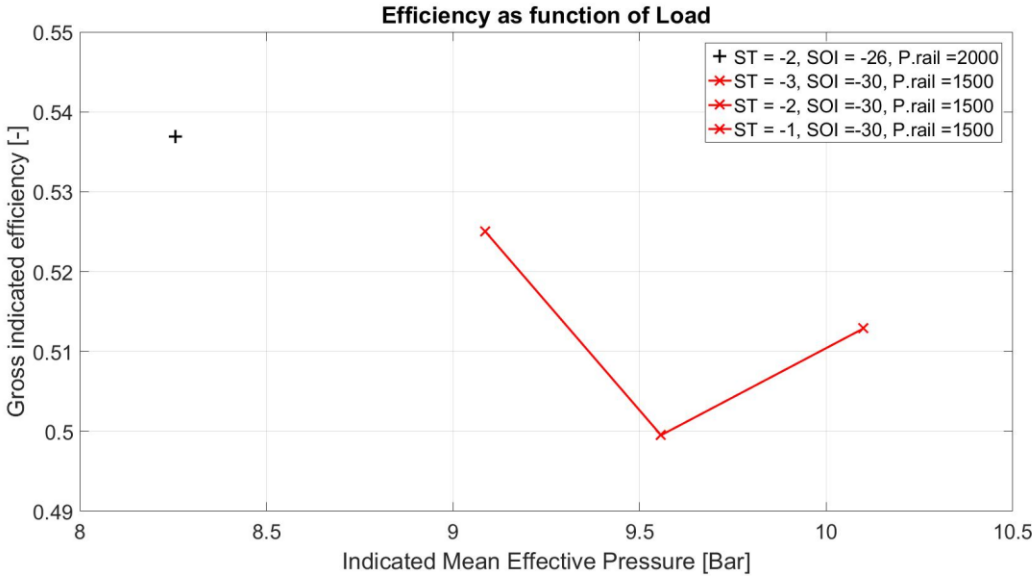

Figure 56

Chapter 8

8 CONCLUSION

At the highest common rail pressure, of 2000 bar, it was possible to maintain stable combustion for a larger range of SOI to ST separation. A lower rail pressure also correlates to optimal spark timing advancement

A large charge air cooling effect is apparent on the cylinder pressure traces due to a combination of a higher heat of vaporisation, a low lower heating value, and a higher stoichiometric equivalence ratio.

The heat release curves for this combustion concept have an unusual shape, not recognisable from either typical diesel CI or gasoline SI combustion. This is most likely due to the flame propagation around the piston bowl. Where the flame area is thought to steadily increase until it meets the pip where the flame area is reduced, before coming around the pip, where it can then increase once again.

Optimal SOI to ST separation at P.rail = 2000 bar was between 23 and 25 CAD. Optimal SOI to ST separation at 1500 and 1000 bar rail pressure was 26 CAD. Confirming *hypothesis 1*.

Indicated gross efficiencies of over 45%, common for all common rail pressures. Indicated gross efficiencies over 50% were recorded most often at a common rail pressure of 1000 bar and a spark timing at ST = -4 and -6 CAD. Due to a fuel leak the indicated efficiencies at 2000 bar common rail pressure were not reliably recorded. The highest recorded gross indicated efficiency was 54%.

Globally lean mixtures are optimal, ensuring sufficient oxygen in the piston bowl for good flame propagation, higher combustion efficiency, reduced CO emissions and an optimal burn duration.

Overall EGR with optimised combustion phasing has the effect of; reducing NOx levels confirming *Hypothesis 3*, although similar specific NOx emissions were recorded without EGR, producing low specific HC and CO emissions confirming *Hypothesis 4*, again similar results were achieved without EGR. At EGR levels above 20% relatively high levels of HC and CO emissions were recorded, confirming *Hypothesis 5*, together with a reduced gross indicated efficiency.

Increasing EGR levels delays combustion phasing and duration which leads to increased expansion work losses. Increased EGR also leads to reduced combustion temperatures which should reduce heat transfer losses. The combination of these to effects causes a reduction in indicated efficiency.

Optimal spark timing to start of injection separation should be reduced as EGR additions increase. Confirming *Hypothesis 2.* As EGR has the effect of retarding flame propagation leading to a longer combustion duration. Advancing the spark timing has the effect of advancing combustion phasing in order to reduce the amount of lost work caused by the expanding cylinder volume. Making it possible to achieve good specific engine-out emissions combined with gross indicated efficiencies of 47% at 20% EGR.

Overall this combustion concept produced unexpectedly high combustion efficiencies, much better than standard PFI SI combustion disproving *Hypothesis 7.* Specific engine-out emissions were outside of current EURO VI regulations for most operational points, an emission after treatment system would be required, disproving *Hypothesis 6.* Additional heating of the intake air was required for combustion.

Chapter 9

9 SOURCES OF ERROR

The credibility of this report is dependent upon the accuracy of the measurement. Two main sources of error have been identified by the author.

Firstly, the fuel measurement system. Fuel is contained in a vessel which hangs on a scale. Fuel is then circulated to the common rail and is cooled before it returns to the main vessel. The scale takes fuel measurements every two seconds. The error of this system is regarded to be very small.

Secondly, the total hydrocarbon emissions. The recorded emission levels HC have two possible sources of error. The AVL emission system used may have reduced sensitivity recording methanol. Also it is possible that unburned hydrocarbons could oxidise in the exhaust manifold before they reach the sensor. Both of these errors would result in recording a higher combustion efficiency. Again the scale of these errors is regarded to be negligable.

Chapter 10

10 BIBLIOGRAPHY

[1] "The Paris Agreement," 14 November 2016. [Online]. Available: http://unfccc.int/paris_agreement/items/9485.php.

[2] "SUMMETH - Sustainable Marine Methanol," SSPA Sweden AB, 2016. [Online]. Available: http://www.sspa.se/alternative-fuels/methanol-alternative-fuel-smaller-vessels.

[3] E. R. Palmer, "Gasification of Wood For Methanol Production," *Energy in Agriculture,* vol. 3, pp. 363-375, 1984.

[4] R. Pearson, M. Eisman, J. Turner, P. Edwards, Z. Jiang, V. Kuznetsov, K. Littau, L. di Marco and S. Taylor, "Energy Storage via Carbon-Neutral Fuels Made From CO2, Water and Renewable Energy," *Proceedings of the IEEE,* vol. 100, no. 2, pp. 440-460, Febuary 2012.

[5] V. Philips and P. Takahashi, "Methanol from biomass," *Environ. Sci. Technol.,* vol. 24, no. 8, pp. 1136-1137, 1990.

[6] B. Johansson, Combustion Engines, Lund: Lund University, Faculty of Engineering, Division of Combustion Enignes, Department of Energy Sciences, 2014.

[7] K. Steurs, C. K. Blomberg and K. Boulouchos, "Knock in an Ethanol Fueled Spark Ignition Engine: Detection Methods with Cycle-Statistical Analysis and Prediction Using Different Ignition Models," SAE Technical Paper 2014-01-1215, 2014.

[8] J. B. Heywood, Internal Combustion Engine Fundamentals, McGraw-Hill Book Company, 1988.

[9] L. J. Hamilton, M. G. Rostedt, P. A. Caton and J. S. Cowart, "Pre-Ignition Characteristics of Ethanol and E85 in a Spark Ignition Engine," SAE Technical Paper 2008-01-0321, 2008.

[10] J. Vancoillie, J. Demuynck, L. Sileghem, M. Van De Ginste, S. Verhelst, L. Brabant and L. Van Hoorebeke, "The potential of methanol as a fuel for flex-fuel and dedicated spark-ignition engines," *Applied Energy,* vol. 102, pp. 140-149, 2013.

[11] M. J. Brusstar and C. L. Gray, Jr., "High Efficiency with Future Alcohol Fuels in a Stoichiometric Medium Duty Spark Ignition Engine," SAE Technical Paper 2007-01-3993, 2007.

[12] L. Sileghem, A. Ickes, T. Wallner and S. Verhelst, “Experimental Investigation of a DISI Production Engine Fuelled with Methanol, Ethanol, Butanol and ISO-Stoichiometric Alcohol Blends,” SAE Technical Paper 2015-01-0768, 2015.

[13] M. Brusstar, M. Stuhldreher, D. Swain and W. Pidgeon, “High Efficiency and Low Emissions from a Port-Injected Engine with Neat Alcohol Fuels,” SAE Technical Paper 2002-01-2743, 2002.

[14] C. Li, L. Yin, S. Shamun and M. Tunér, “Transistion from HCCI to PPC: The Sensitivity of Combustion Phasing to the Intake Temperature and the Injection Timing with and without EGR,” SAE Technical Paper, 2016-01-0767.

[15] “Diesel.net,” 11 2016. [Online]. Available: https://www.dieselnet.com/standards/eu/hd.php. [Accessed 06 04 2017].

[16] K. Naganuma, J. Vancoillie, L. Sileghem and S. Verhelst, “Drive Cycle Analysis of Load Control Strategies for Methanol Fuelled ICE Vehicle,” SAE Technical Paper 2012-01-1606, 2012.

[17] J. Vancoillie, J. Demuynck, L. Sileghem, M. Van de Ginste and S. Verhelst, “Comparison of the renewable transportation fuels, hydrogen and methanol formed from hydrogen, with gasoline - Engine efficiency study,” *International Journal of Hydrogen Energy*, vol. 37, pp. 9914-9924, 2012.

Chapter 10

10 LIST OF FIGURES